Simulation & Epitaxial Growth of AlN/GaN Nano-Heterostructures for High Electron Mobility Transistors

Master of Science (MSc) in Photonics & Nanoelectronics

Physics Department, University of Crete

Institute of Electronic Structure & Laser - FORTH

Thesis by

Antonios I. Bairamis

Committee in charge

Prof. Alexandros Georgakilas (supervisor)

Prof. Eleftherios Iliopoulos

Dr. George Konstantinidis

Τριμελής εξεταστική επιτροπή

Αλέξανδρος Γεωργακίλας (επιβλέπων καθηγητής)

Ελευθέριος Ηλιόπουλος (καθηγητής)

Γεώργιος Κωνσταντινίδης (ερευνητής)

Heraklion, 12th of December 2018

Ηράκλειο, 12 Δεκεμβρίου 2018

To my parents and probabilities

Στους γονείς μου και την πιθανοκρατία

Contents

Summary / Περίληψη

The study of the electrical and optical properties of solids, especially of semiconductors, is undoubtedly a major and influential subject of modern physics. Semiconductor physics has given us the ability to construct complex materials and structures, which do not exist in nature and have various desirable properties, and all that in a scale of just a few nanometers. The family of III-V compound semiconductors, in particular, is known for its high electron mobilities and direct band gaps. The last twenty years we have witnessed the flare of the group-III nitride semiconductors (GaN, InN, AlN) and their alloys. The strong polarization effects in III-nitrides (of wurtzite structure) induce high electric fields in their heterostructures that enable the high carrier concentration and spatial confinement of the 2-Dimensional Electron Gas (2DEG). The 2DEG serves as a conduction channel that facilitates a high current density in HEMTs. The present thesis focuses on the design and growth optimization of the AlN/GaN HEMT heterostructure and the ability of achieving high electron density and mobility values. Moreover, Self-Consistent Schrödinger-Poisson (SCSP) calculations and experiments of epitaxial growth and characterization of AlN/GaN/AlN HEMT double heterostructures (DHs) were carried out. Finally, we tried to provide an insight into GaN and AlN surface passivation, using an *in-situ* SiN_x cap layer grown by plasma-assisted molecular beam epitaxy (PAMBE).

The work has been carried out within the **NITROHEMT** project of the **ARISTEIA** program and was co-funded by the *European Social Fund (ESF)* and *National Resources*. Special thanks to Prof. A. Georgakilas and to Ch. Zervos, A. Adikimenakis and K. Tsagaraki for their valuable help and collaboration.

Η μελέτη των ηλεκτρικών και οπτικών ιδιοτήτων των στερεών, ιδιαίτερα των ημιαγωγών, είναι αναμφισβήτητα ένα σημαντικό και με επιρροή θέμα της σύγχρονης φυσικής. Η φυσική των ημιαγωγών έχει δώσει τη δυνατότητα να κατασκευαστούν σύνθετα υλικά και δομές που δεν υπάρχουν στη φύση και έχουν διάφορες επιθυμητές ιδιότητες, και όλα αυτά σε κλίμακα μόλις μερικών νανομέτρων. Ειδικότερα, η οικογένεια των σύνθετων ημιαγωγών III-V είναι γνωστή για τις υψηλές ευκινησίες ηλεκτρονίων και τα άμεσα ενεργειακά χάσματα. Τα τελευταία είκοσι χρόνια παρατηρούμε την ανάπτυξη των ημιαγωγών νιτριδίων (GaN, InN, AlN) και των κραμάτων τους. Τα ισχυρά φαινόμενα πόλωσης στους ημιαγωγούς νιτριδίων εισάγουν υψηλά ηλεκτρικά πεδία στις διεπιφάνειες των ετεροδομών που επιτρέπουν την υψηλή συγκέντρωση ηλεκτρονίων και την δημιουργία διδιάστατου ηλεκτρονικού αερίου (2DEG). Το 2DEG χρησιμεύει ως κανάλι αγωγιμότητας που διευκολύνει την υψηλή πυκνότητα ρεύματος στα Τρανζίστορ Υψηλής Ευκινησίας (HEMT). Η παρούσα εργασία επικεντρώνεται στη βελτιστοποίηση του σχεδιασμού και της ανάπτυξης της απλής ετεροδομής AlN/GaN HEMT και στην ικανότητα επίτευξης υψηλών τιμών συγκέντρωσης ηλεκτρονίων και ευκινησίας. Επιπλέον, πραγματοποιήθηκαν υπολογισμοί SCSP και πειράματα επιταξιακής ανάπτυξης και χαρακτηρισμού των διπλών ετεροδομών HEMT AlN/GaN/AlN. Τέλος, προσπαθήσαμε να δώσουμε μια εικόνα για την προστασία και αδρανοποίηση των επιφανειών GaN και AIN, χρησιμοποιώντας ένα στρώμα μονωτικού νιτριδίου του πυριτίου (SiN_x) που αναπτύχθηκε μέσα στον θάλαμο του MBE (in-situ).

Οι εργασίες πραγματοποιήθηκαν στο πλαίσιο του προγράμματος **NITROHEMT** του προγράμματος **ΑΡΙΣΤΕΙΑ** που συγχρηματοδοτήθηκε από *Ευρωπαϊκό Κονδύλιο* και *Εθνικούς Πόρους*. Ιδιαίτερες ευχαριστίες στον καθηγητή Α. Γεωργακίλα και στους Χ. Ζερβό, Α. Αδικιμενάκη και Κ. Τσαγκαράκη για την πολύτιμη βοήθεια και συνεργασία τους.

❖

Chapter 1

Introduction

The study of the electrical and optical properties of solids, especially of semiconductors, is undoubtedly a major and influential subject of modern physics. But it is also a field of science where basic research and technology tend to evolve in a parallel way with very close interaction. In the second half of the 20th century this parallel evolvement gave, and continues giving, impressive results concerning the field of condensed matter physics. Especially, semiconductor physics and its impressive technological achievements of the recent past years, have given the ability to construct complex semiconductor materials and structures, which do not exist in nature and have various desirable properties, and all that in a scale of just a few nanometers.

Due to rapid progress in technology and the progressively shrinking dimensions of several devices to the nanometer scale (one nanometer (nm) is one billionth, or 10^{-9}, of a meter), many of the classical assumptions become invalid and must be discarded in favor of a more quantum mechanical description (nanosciences). The modern solid state physics is, to a large extent, the application of quantum mechanics and statistical mechanics to the study of electronic structure of solids. The use of quantum mechanics has allowed a very good understanding of the properties of different types of solid materials such as metals, semiconductors, superconductors and magnetic materials. For instance, the electronic states in highly confined semiconductor structures, like quantum dots, are entirely controlled by quantum mechanical size quantization, which can be exploited for entirely new device designs like quantum well or quantum dot lasers.[1]

At the same time, the physical equations that describe these quantum systems are much too complex to be solved analytically and efficient numerical solution methods need to be used instead.

1.1 Semiconductor Technology

Semiconductor materials have fueled many technological breakthroughs over the last half century (high speed wireless communications, computing, solid-state lighting, solar powering, high power electronics, etc.)[2], having a monumental impact on our society. Switching, amplification and light-electricity conversion are the most important functions they perform.

The family of III-V compound semiconductors, in particular, is known for its high electron mobilities and direct band gaps. Most importantly, they are versatile materials due to the possibility to tailor their (opto) electronic properties by selecting their composition appropriately. When grown heteroepitaxially, though, this possibility is constrained by the lattice mismatch with the substrate. The situation is significantly different in epitaxial nanostructures, where more possibilities for strain engineering are offered at the nanoscale and new physical phenomena with potential device applications can be explored. On the other hand, the growth of such nanostructures is very demanding and necessitates good understanding and precise control of the growth mechanisms.

The last twenty years we have witnessed the flare of the group-III nitride semiconductors (GaN, InN, AlN) and their alloys. The premature nature of these wide bandgap materials (see Fig. 1.1), in spite of a number of defects, has made possible the demonstration of the most efficient blue-laser diode[3] and the highest output power-density from any field-effect transistor.[4]

It has been accepted for a couple of years that III-N based High-Electron Mobility Transistors (HEMTs) are becoming the "toughest transistors yet" because of their capability for unprecedented power performance.[5]

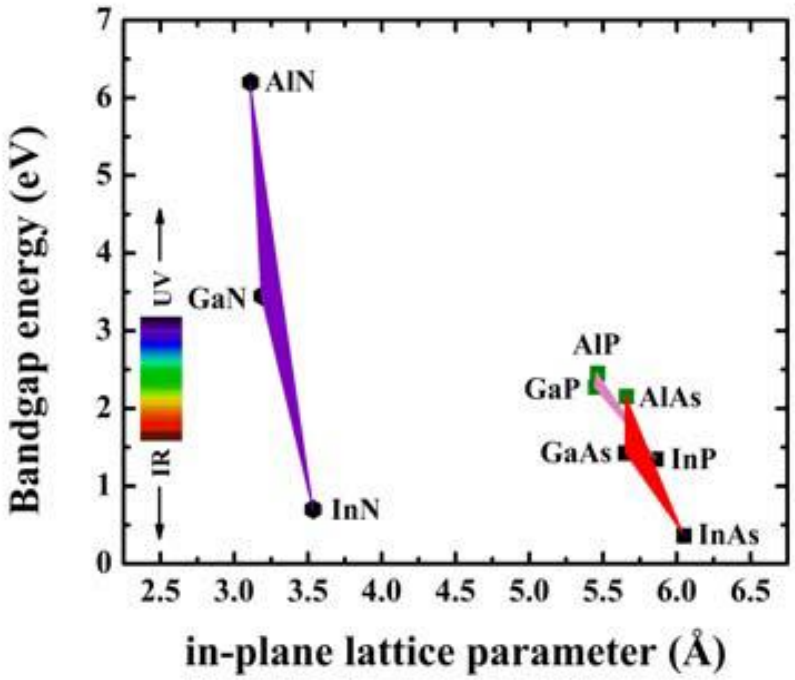

Fig. 1.1. Band gap energies of the most important semiconductors as a function of their lattice parameter. The right-hand scale gives the light wavelength (λ), corresponding to the band gap energy *[Figure taken from E. Dimakis' PhD Thesis]*.[6]

The strong polarization effects in III-nitrides (of wurtzite structure) induce high electric fields in their heterostructures that enable the high carrier concentration and spatial confinement of the 2-Dimensional Electron Gas (2DEG). The 2DEG serves as a conduction channel that facilitates a high current density in HEMTs. The electron density is mainly determined by

conduction band offset and the polarization discontinuity at the III-Nitrides' heterojunction, without the need of incorporating donor dopants in the (larger bandgap) barrier layer. The discontinuity of polarization at the AlGaN/GaN heterojunction, for example, has been found to induce a two-dimensional electron gas (2DEG) of high density[7] ($N_S = 10^{13}\,cm^{-2}$). Such 2DEGs have been used as the channel material[8] for field-effect transistors (FETs) that are commonly called HEMTs.

High electron mobility transistors (HEMTs belong to the more general class of Heterostructure FETs, HFETs) have proliferated themselves as the preferred transistor type for RF and microwave frequency applications, especially when high power outputs are required. The basic structure of such transistors consists of a very thin barrier layer of a group III-nitride ($Al_xGa_{1-x}N$ or $In_xAl_{1-x}N$), usually with thickness in the range of 3-30 nanometers, above a lower bandgap GaN layer. Double barrier structures, where the lower bandgap GaN layer is sandwiched between two larger bandgap barrier layers are also possible. The bandgap difference between these layers will play a major role in the working of the transistor. The double heterostructure with a thin GaN layer is called a quantum well. Varying certain structure parameters such as the composition of the AlGaN barrier layers, the well width and bandgap discontinuity, we can modify and control factors such as carrier confinement and transition energy of quantum wells which invariably controls the output of the devices.[9]

1.2 Purpose of the thesis

The present thesis focuses on the design and growth optimization of the AlN/GaN HEMT heterostructure and the ability of achieving high electron density and mobility values. Initial work aimed to the optimization of the single AlN barrier HEMT structure (single AlN/GaN heterostructure). More specifically, theoretical calculations were used to investigate the effect of a GaN coating (cap) layer on the AlN barrier layer and mostly on the sheet charge density (Ns) of the 2DEG, which is affected by the negative polarization charge at the upper GaN/AlN interface. This is done through the numerical solution of a self-consistent Schrödinger-Poisson system (SCSP)[10] incorporating the polarization effects. Additionally, Hall-effect measurements were carried out in order for the electrical properties of the heterostructures to be investigated. Subsequently, SCSP calculations and experiments of epitaxial growth and characterization of AlN/GaN/AlN HEMT double heterostructures (DHs), with 1 nm GaN cap and different thicknesses (t_b) of AlN barrier layer, have taken place (Chapter 5.2). Although these structures with high 2DEG densities can be successfully grown,[11,12] the existing trapping effects may limit the performance of the fabricated devices through drain-current collapse.[13] The reduction of surface states and sheet resistance, which is favorable for a device operation, is feasible using different passivation layers or gate insulators. We tried to provide an insight into GaN and AlN surface passivation, using an *in-situ* SiN_x cap layer grown by plasma-assisted molecular beam epitaxy (PAMBE). The HEMT structures (passivated and unpassivated) were analyzed both theoretically and experimentally, and the effect of SiN_x cap layer on the 2DEG density was evaluated (Chapter 5.3).

Sententiously, this thesis discusses the physical properties of group-III nitrides in Chapter 2, followed by the report of growth and characterization techniques in Chapter 3. The Schrödinger-Poisson theory and the materials parameters used in the calculations are given in Chapter 4. The subsequent experimental and calculated results, as well as a discussion about them, are shown in Chapter 5. This report is concluded in Chapter 6 by giving an outlook based on the conclusions reached in this work.

References

[1] P. Harrison, *Quantum Wells, Wires and Dots – Theoretical and Computational Physics of Semiconductor Nanostructures*, Wiley-Interscience Publications, Chapter 8 (2005)

[2] S. C. Jain, M. Willander, J. Narayan & R. V. Overstraeten, *J. Appl. Phys.* **87**, p. 965 (2000)

[3] S. Nakamura, M. Senoh, A. Nagahama, N. Iwasa, T. Yamada, T. Matsushita, H. Kiyoku & Y. Sugimoto, *Jpn. J. Appl. Phys.* **35**, Part 2, p. L 74 (1996)

[4] U. K. Mishra, P. Parikh & Y. F.Wu, *Proceedings of the IEEE.* **90**, p. 1022 (2002)

[5] L. F. Eastman & U. K. Mishra, *IEEE Spectr.* **39**, no. 5, pp. 28–33 (2002)

[6] E. Dimakis, *Physical Mechanisms in Molecular Beam Epitaxy and Properties of InN (0001) Films*, PhD Thesis, University of Crete (2007)

[7] O. Ambacher, B. Foutz, J. Smart, J. R. Shealy, N. G.Weimann, K. Chu, M. Murphy, A. J. Sierakowski, W. J. Schaff, L. F. Eastman, R. Dimitrov, A. Mitchell & M. Stutzmann, *J. Appl. Phys.* **87**, p. 334 (2000)

[8] Y. F. Wu, B. P. Keller, P. Fini, S. Keller, T. J. Jenkins, L. T. Kehias, S. P. DenBaars & U. K. Mishra, *IEEE Electron Device Lett.* **19**, p. 50 (1998)

[9] J. Piprek, *Nitride Semiconductor Devices: Principles and Simulation*, Wiley-VCH Verlag, Chapter 10 (2007)

[10] I-H. Tan, G.L. Snider, L.D. Chang & E.L. Hu, *J. Appl. Phys.* **68** (8), 4071-4076 (1990)

[11] A. Bairamis, Ch. Zervos, A. Adikimenakis, A. Kostopoulos, M. Kayambaki, K. Tsagaraki, G. Konstantinidis & A. Georgakilas, *Appl. Phys. Lett.* **105**, 113508 (2014)

[12] A. Adikimenakis, K.E. Aretouli, E. Iliopoulos, A. Kostopoulos, K. Tsagaraki, G. Konstantinidis & A. Georgakilas, *Microelectron. Eng.* **86**, 1071 (2009)

[13] S. Arulkumaran, T. Egawa, H. Ishikawa & T. Jimbo, *Appl. Phys. Lett.* **81**, 3073 (2002)

Chapter 2

Properties of Group-III Nitrides

Group-III nitrides refer to the compound semiconductors composed of a group-III element(s) (Al, Ga, In) and Nitrogen (N) and their associated alloys.[1] Some of the characteristics with unique merit are their wide energy bandgaps and a wurtzite crystal structure which bring about significant polarization effects. GaN and $Al_xGa_{1-x}N$ have proliferated themselves amongst the III-nitrides for technological reasons but other III-nitrides like $In_xGa_{1-x}N$ may prove superior in FET applications if the technological issues can be cured that arise due to the big difference in ionic size of In and N.[1] Quaternary alloys, like $In_xAl_yGa_{1-(x+y)}N$, provide an extra degree of freedom that allow manipulating the energy bandgap and lattice constants of the material independently. The problem is that these kinds of alloys are hard-growing materials because of the significantly weaker (and longer) In-N bonds[1] and the epitaxial growth of InN at approximately half of the growth temperatures used for GaN and AlN binaries.

2.1 Crystal Structure

The group-III nitrides may occur in either a wurtzite (hexagonal) or a zincblende (cubic) crystal structure with the former being the thermodynamically most stable form at room temperature.[2] The wurtzite crystal structure has a hexagonal unit cell, with lattice constants *a* and

c, formed by two interpenetrating hexagonal close-packed (hcp) sublattices (see Figure 2.1). Each sublattice consists of either group-III element or nitrogen forming cations and anions, respectively. Each nitrogen (group III) atom is coordinated by four group-III (nitrogen) atoms. Figure 2.1 shows this tetrahedral arrangement with the cation-anion bonds. The nonsymmetric offset, between the sublattices along the c-axis, makes the GaN epitaxial layers commonly grown along the {0001} basal plane, either Ga-faced or N-faced giving a polarity to the surface of the material. Each polar surface has unique chemical and physical properties. The polarity of the epitaxial layers is not predicted easily for a specific deposition technique and should be verified with experiment for every structure.[3]

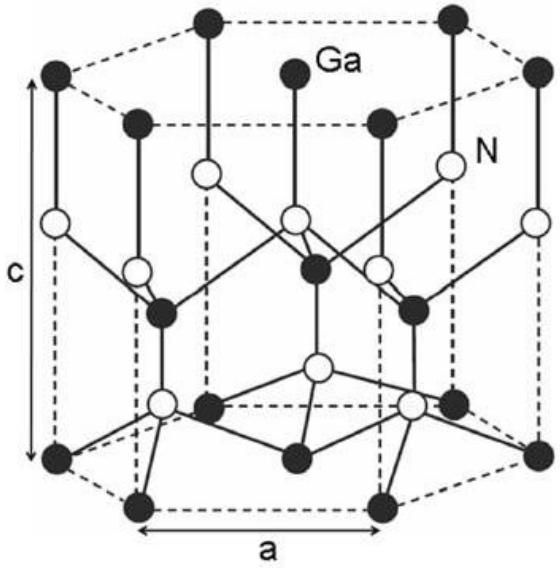

Fig. 2.1. Wurtzite crystal structure of GaN. The structure is formed by two intertwined hexagonal sublattices of Ga and N atoms *[Figure taken from Piprek's book "Nitride Semiconductor Devices: Principles and Simulation", Wiley-VCH Verlag].*[2]

2.2 Polarization in III-Nitrides

The group-III nitrides are distinguishable among the III-V semiconductors because nitrogen is the smallest and most electronegative of the group-V elements. The metal-nitrogen covalent bond has a greater degree of ionicity than other III-V covalent bonds.[3] This dipole can induce a net polarization across a macroscopic layer if the symmetry of the crystal allows it. In wurtzite III-V nitride semiconductors the atomic crystal arrangement is such that a net dipole moment is present even under no applied strain.[3,4] Since this polarization effect occurs in the equilibrium lattice of the III-N at zero strain, it is termed **spontaneous polarization, P_S**.[5,6] The degree of non-ideality of the crystal lattice governs the strength of the spontaneous polarization. All III-nitrides have a negative value for P_S[5] (taking the direction along the c-axis, [0001], as positive).

In addition to the spontaneous polarization presence in wurtzite III-V semiconductors, there is also a piezoelectric component caused by strain. **Piezoelectric polarization, P_{PZ}**, refers to the polarization induced by a mechanical strain[5,6] in a material and can be many times larger in the nitrides as compared to other compound semiconductors.[1] A strain in the (0001) plane, either compressive or tensile, changes the bond angles of atoms and thereby a dipole moment arises along the [0001] directions.

The P_S in a given material is constant, while the P_{PZ} is a function of strain and can be calculated from:[5]

$$P_{PZ} = 2\left(e_{31} - e_{33}\frac{C_{13}}{C_{33}} \right)\varepsilon \qquad (2.1)$$

where e_{31}, e_{33} are the piezoelectric coefficients, C_{13}, C_{33} are the elastic constants, and ε is the in-plane strain in the crystal given by:

$$\varepsilon = \frac{\alpha - \alpha_0}{\alpha_0} \qquad (2.2)$$

where α, α_0 are the lattice constants of the strained layer and the substrate, respectively.

In wurtzite III-N, e_{31} is always negative while e_{33}, C_{13} and C_{33} are always positive, therefore the bracket in Equation 2.1 will always be a negative number.[3] As a consequence, P_{PZ} is always negative for layers under tensile stress ($\alpha > \alpha_0$) and positive for layers under compressive stress ($\alpha < \alpha_0$). Noting that P_S is always negative in III-N, P_S and P_{PZ} are parallel to each other, for layers under tensile stress, and in those under compressive stress the two polarizations are anti-parallel.[4] Table 2.1 shows the mechanical[3,5] and piezoelectric constants,[6,7] as well as the spontaneous polarization,[3,5] for the three binary nitride semiconductors. Material properties of ternary alloys can be determined by linearly interpolating these constants[3] (see Chapter 4).

Material	α_0 (Ang)	Gap (eV)	P_{SP} (C/m²)	e_{31} (C/m²)	e_{33} (C/m²)	C_{13} (GPa)	C_{33} (GPa)
GaN	3.1986	3.42	-0.034	-0.34	0.67	68	354
AlN	3.1095	6.28	-0.090	-0.53	1.50	94	377
InN	3.5848	~ 0.63	-0.042	-0.41	0.81	70	205

Table 2.1. Nitride material parameters.

2.2.1 Polarization-Induced n-type Doping

Polarization field creates fixed charges at the interface between two layers of different nitride materials.[3] These charges can be used to enhance the carrier concentration of many devices without the need for introducing any impurity dopants into the crystal. The absence of dopants in the material enhances the carrier mobility by reducing impurity scattering.[3] This is something of maximum importance in devices like HEMTs where high mobilities of electrons are critical for high-speed operation. Polarization charges can be calculated by using Gauss's law:

$$\nabla \cdot D = \rho_{fixed} + \rho_{mobile} \qquad (2.3)$$

where ρ_{fixed} is the total fixed volume charge concentration, ρ_{mobile} is the mobile charge density, and D is the electric displacement. The total fixed charge is related to the total polarization of the crystal, P, by:

$$\rho_{fixed} = -\nabla \cdot P \qquad (2.4)$$

Equation 2.4 shows that a spatially changing polarization field creates a net bound charge in the crystal. This charge is referred to as polarization charge, is fixed in space and it can induce mobile carriers of the opposite sign, as is explained below.

2.2.2 Two-Dimensional Electron Gas (2DEG)

In the simplest case, where polarization fields change abruptly across a sharp heterojunction, Maxwell's equations are reduced[3] to:

$$q\sigma_{pol} = \hat{n} \cdot \left(P_1 - P_2 \right) \quad (2.5)$$

where σ_{pol} is the sheet charge concentration at the heterojunction interface (cm^{-2}), P_1, P_2 are the total polarization of first and second layer respectively, and $\hat{n}$ is the unit vector normal to the interface.

When a thin $Al_xGa_{1-x}N$ layer is epitaxially grown on Ga-face GaN a two-dimensional electron gas (2DEG) results at the heterojunction.[3] The polarization induced charge at the AlGaN/GaN heterojunction is neutralized by mobile electrons that are attracted from the semiconductor surroundings and tend to accumulate near the interface adding to the 2DEG density. These mobile electrons are then used as the conduction channel in a HEMT. The need for modulation doping does not exist here. The 2DEG density in polarization-induced 2DEGs is generally determined by the composition and thickness of the layers comprising the HEMT heterostructure, i.e. thickness and composition (x) of $Al_xGa_{1-x}N$ barrier in the case of $Al_xGa_{1-x}N$/GaN HEMTs. The strength of the polarization field is controlled by the composition, and the magnitude of the band-bending, that results from the polarization charges, is directly dependent on the thickness of layers.[8] By combining Equations 2.1 and 2.5, for the two different epitaxial layers of an AlGaN/GaN heterojunction, we can write:[3]

$$q\sigma_{pol} = \left[\Delta P_{SP} + 2\left(e_{31} - e_{33}\frac{C_{13}}{C_{33}} \right)\left(\frac{\alpha_{AlGaN} - \alpha_{GaN}}{\alpha_{GaN}} \right) \right] \quad (2.6)$$

where ΔP_{SP} is the difference in spontaneous polarization between the GaN and the AlGaN layer.

Figure 2.2 shows the structure of a typical AlGaN/GaN HEMT.[8] A high-density 2DEG forms at the AlGaN/GaN heterojunction due to the discontinuity in polarization across the heterointerface.

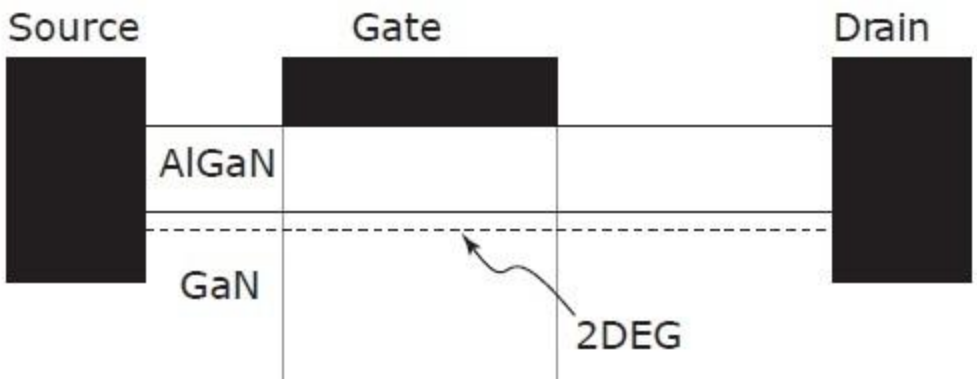

Fig. 2.2. Structure of an AlGaN/GaN HEMT, showing the 2DEG at the heterointerface. *[Figure taken from the book "Polarization Effects in Semiconductors", eds. C. Wood & D. Jena, Springer].*[8]

The electron concentration at the AlGaN/GaN interface can be determined by a calculation of the band diagram using a self-consistent Schrödinger Poisson solver.[9] Figure 2.3 shows the conduction band diagrams and the electron concentrations of three random GaN/AlN/GaN structures.

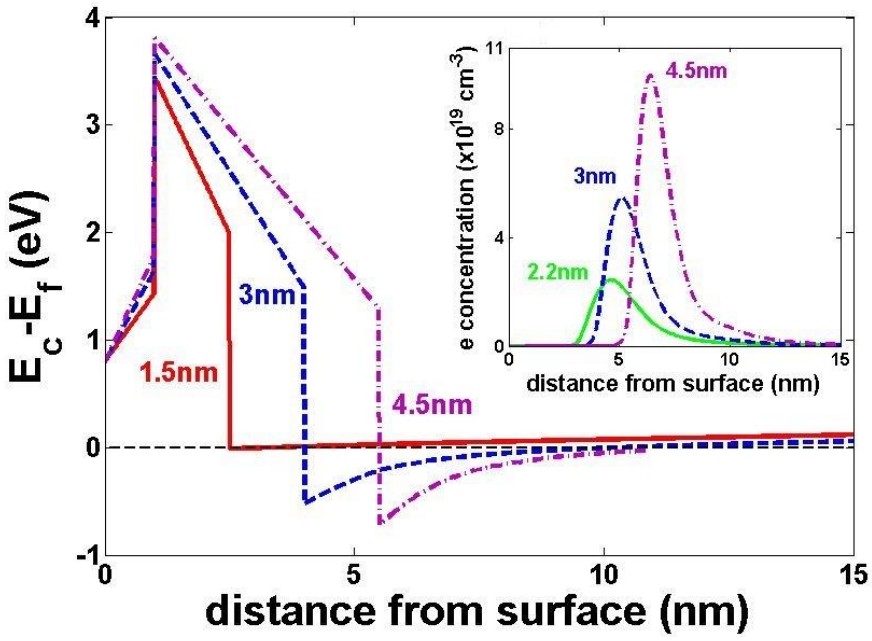

Fig. 2.3. Simulated conduction band diagrams and electron concentrations of three random GaN/AlN/GaN structures using self-consistent Schrödinger-Poisson calclulations.

2.3 Applications of Nitrides

Nitride related compound semiconductors have been the most attractive materials in optoelectronic devices for short wavelength emission.[1] The bandgap of nitride compounds including InN, GaN, AlN, and their alloys, cover wide ranges from ~0.63 to 6.2 eV, which cover infrared to ultraviolet emission spectrum. Therefore, they have been widely applied in blue and ultraviolet emission devices such as laser diodes.[10]

In addition to applications in optoelectronics, nitrides are also very important materials for high power electronic applications. Extremely high 2DEG densities can be achieved (N_S ~ 10^{13} cm^{-2}) with reasonably high room temperature mobility (μ ~ 1500 cm^2/Vs). Such properties

make the AlGaN/GaN heterojunction 2DEG suitable for field-effect transistors used as switches in power electronic circuits of voltage inverters and converters or for generation and amplification of RF waves/signals in integrated circuits for radars and telecommunications.[8] Table 2.2 shows a material properties comparison to the current available technologies. Si and GaAs are the basis of the most matured technologies in the market. However, Si and GaAs have relatively small band gaps and low saturation velocities in high field region. The breakdown fields for Si and GaAs are also smaller compared to the wide bandgap semiconductors listed in Table 2.2 and therefore, these devices are only suitable for low power and high speed device applications.[10]

	Si	GaAs	Diamond	SiC	GaN
μ (cm^2/Vs)	600	8500	2200	1000	1600
Eg (eV)	1.12	1.43	5.45	3.26	3.40
v_{sat} (10^7 cm/s)	1.0	1.0	2.7	2.0	2.0
E_{break} (kV/cm)	300	400	10,000	2,200	2,000
Thermal conductivity (W/cmk)	1.5	0.46	22.0	4.40	2.30

Table 2.2. Material comparison for high power high frequency operation *[Table taken from Wu et al]*[10].

2.4 Defects and Scattering Mechanisms

All real crystals contain imperfections (defects) which may be point, line (dislocations), surface or volume defects, and which disturb locally the regular arrangement of the atoms.[11] *Dislocations* are an important class of defects and their presence can significantly modify the properties of crystalline solids.[11] Moreover, the absence of native substrates has notable implications for III-N devices technology due to the lattice and thermal mismatch. The heteroepitaxial nature of most nitride semiconductors leads to the presence of very high dislocations densities (typically in the range of $10^8 – 10^{10}$ cm^{-2}).[4]

Electrons moving in a 2DEG channel experience *interface-roughness scattering*[8] due to the non-abrupt interface between AlGaN and GaN. The 2DEG wavefunction is mostly confined in GaN, but there is a finite part that penetrates the AlGaN barrier, leading to *alloy-disorder scattering*.[8] These two types of scattering are short-range. But, there are also long-range (Coulombic) scattering sources, constituted by the presence of charged impurities or defects in the samples, like *dislocation scattering*. Also, *trap centers*, whose energy levels lie in the forbidden gap, exchange charge with the conduction and valence bands through the emission and capture of electrons. The trap centers change the density of space charge in semiconductor bulk and influence the recombination statics.[10] Finally, *dipole scattering* which is a dominant mechanism and originates in the AlGaN/GaN system due to the coupling of alloy disorder in the barrier and the strong polarization of the material system.[8]

All the above phenomena, combined with the a priori difficulties of growing heteroepitaxial thin films, are reasons for limiting the high performance of III-nitride based heterostructures devices.

References

[1] H. Morkoc, *Handbook of Nitride Semiconductors and Devices: Electronic and Optical Processes in Nitrides Vol. 1: Materials Properties, Physics and Growth*, Weinheim Wiley-VCH (2008)

[2] J. Piprek, *Nitride Semiconductor Devices: Principles and Simulation*, Wiley-VCH Verlag (2007)

[3] O. Ambacher & V. Cimalla *in Polarization Effects in Semiconductors – From Ab Initio Theory to Device Applications*, Eds. C. Wood & D. Jena, Springer Publications, p. 27-109 (2008)

[4] G. Koley, MVS Chandrashekhar, C. I. Thomas & M. G. Spencer *in Polarization Effects in Semiconductors – From Ab Initio Theory to Device Applications*, Eds. C. Wood & D. Jena, Springer Publications, p. 265-305 (2008)

[5] O. Ambacher et. al., *J. Phys.: Condens. Matter* **14**, 3399-3434 (2002)

[6] F. Bernardini & V. Fiorentini, *Phys. Rev. B* **64**, 85207 (2001)

[7] A. Zoroddu, F. Bernardini, P. Ruggerone & V. Fiorentini, *Phys. Rev. B* **64**, 45208 (2001)

[8] D. Jena *in Polarization Effects in Semiconductors – From Ab Initio Theory to Device Applications*, Eds. C. Wood & D. Jena, Springer Publications, p. 161-216 (2008)

[9] I-H. Tan, G. L. Snider, L. D. Chang & E. L. Hu, *J. Appl. Phys.* **68** (8), 4071-4076 (1990)

[10] Y.-R. Wu, M. Singh & J. Singh *in Polarization Effects in Semiconductors – From Ab Initio Theory to Device Applications*, Eds. C. Wood & D. Jena, Springer Publications, p. 111-159 (2008)

[11] D. Hull & D. J. Bacon, *Introduction to Dislocations*, Butterworth-Heinemann Publications, Elsevier Publishing Group, Chapter 1 (2011)

Chapter 3

Epitaxial Growth & Characterization Methods

3.1 Basics of Molecular Beam Epitaxy (MBE)

The epitaxial growth of semiconductor heterostructures is accomplished by various techniques. The most known are Molecular Beam Epitaxy (MBE), Vapor Phase Epitaxy (VPE) and Liquid Phase Epitaxy (LPE).[1] MBE growth is carried out under conditions far from thermodynamic equilibrium and is governed mainly by the kinetic processes on the substrate surface, which is maintained at an elevated temperature in ultrahigh vacuum, and is subject to the impinging thermal-energy molecular or atomic beams of the constituent elements.[1,2] The atomic beams are created either by sublimation of the components from solid or liquid phase sources (Ga, Al, In, Be, Si, Mg, As), or by using components from gas phase sources (N_2, NH_3). The MBE technique offers absolute growth control and facilitates the study and understanding of natural processes taking part in the growth of semiconductors.[1,2]

In the special case, where plasma gas is used for growth by MBE, the technique is called plasma-assisted MBE (Plasma Assisted MBE, PAMBE). In the present thesis, for the growth of III-nitrides heterostructures, the PAMBE technique was used, employing a radio frequency nitrogen plasma source and evaporation sources (effusion cells) for Ga, Al and In, as shown in Fig. 3.1.[3]

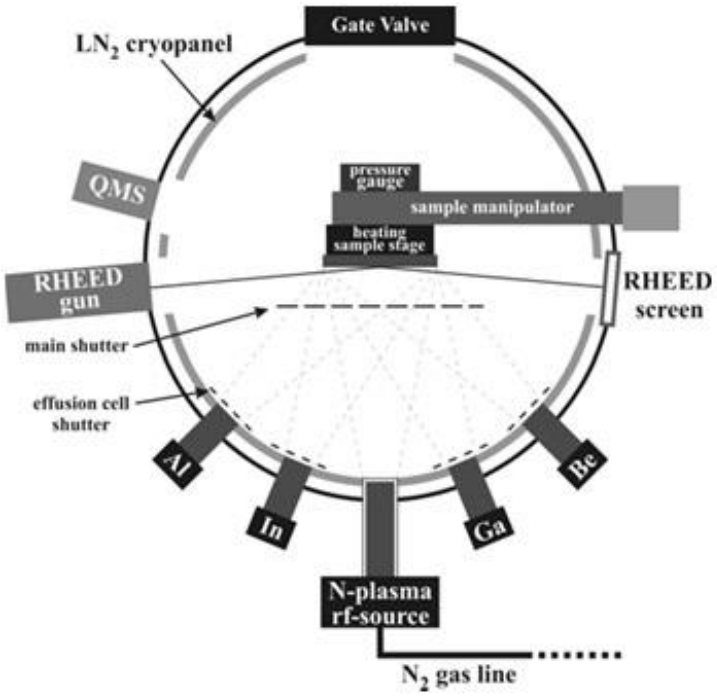

Fig. 3.1. Schematic of the Plasma-Assisted MBE growth chamber that was used for the present thesis.[3]

Being realized in an ultrahigh vacuum environment, MBE processes may be controlled in situ by surface diagnostic methods such as Reflection High-Energy Electron Diffraction (RHEED),[4,5] Auger Electron Spectroscopy (AES) and ellipsometry. These powerful techniques for control and analysis enable the fabrication of sophisticated device structures. The uniformity in thickness as well as in the composition of the layers grown by MBE depends on the uniformities of the molecular beam fluxes and also on the geometrical relationship between the configurations of the sources and the substrate.[1] All the above conditions, plus the fact that the growth becomes layer-by-layer and that results in very smooth surfaces, give to MBE a clear lead over the alternative epitaxial growth techniques. To develop a semiconductor of high crystalline quality, it is desirable to control the processes, by regulating the growth conditions, in

such way that the diffusion of the atoms on the surface is the proper to integrate them into the appropriate crystal lattice points.

A series of surface processes, which are schematically illustrated in Fig. 3.2[3], are involved in MBE growth. Understanding them is of critical importance in order to determine the growth conditions that lead to the best crystalline quality of the epitaxial semiconductor layer. The following are the most important:[1]

- adsorption of the constituent atoms or molecules impinging on the substrate surface,
- surface migration and dissociation of the adsorbed molecules,
- incorporation of the constituent atoms into the crystal lattice of the substrate or the epilayer already grown,
- thermal desorption of the species not incorporated into the crystal lattice.

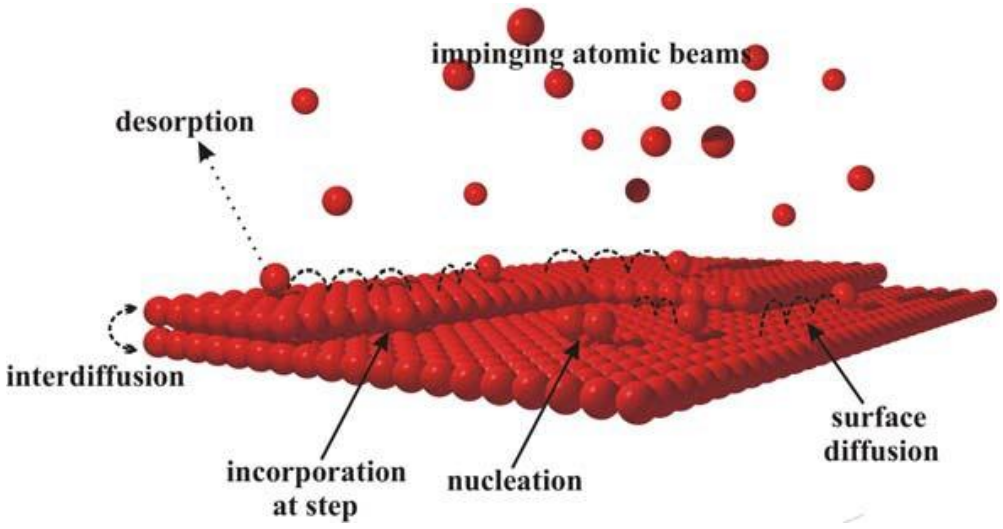

Fig. 3.2. The surface processes that are involved in MBE growth.[3]

3.2 Characterization Techniques

There are two types of characterization tools used to qualify the structural and electronic properties of epitaxial structures. Tools that are used during the epitaxial growth process (*in-situ* techniques), such as Reflection High-Energy Electron Diffraction (RHEED), and post growth tools (*ex-situ* techniques), such as Atomic Force Microscopy (AFM) and resistivity and Hall-effect measurements. A brief overview of these tools is presented in this section.

3.2.1 Reflection High-Energy Electron Diffraction (RHEED)

The Reflection High-Energy Electron Diffraction (RHEED) method is a very important tool for crystal characterization during the growth procedure (in-situ)[4,5] and is based on the diffraction of high voltage electron beam (5-50 keV) from the surface layers of the crystal. RHEED is only used in a MBE system, wherein the growth is carried out under high vacuum conditions and thus the production and propagation of the electron beam in growth chamber are possible. Conversely, the very high pressure in the growth chamber in other techniques makes it impossible to use the RHEED method.

The principle of operation of RHEED is based on the diffraction of high-energy electrons from the two-dimensional periodic lattice of atoms in the surface of a crystal. The electron beam is produced by the electron emission from a heated tungsten (W) filament and its acceleration in a potential difference of 12 kV (RHEED gun). When the electron beam is incident at a very small angle (< 5°), this diffraction occurs from the top few atomic layers of the crystal. After the electron beam is diffracted the diffraction pattern is captured on a fluorescent screen (RHEED screen) and may be recorded with a video camera. The diffraction pattern on the fluorescent

screen indicates the real time smoothness of the surface, as well as the crystal structure of the surface.

In some cases (layer-by-layer growth through nucleation of 2D islands), the intensity of the diffraction pattern can be used to monitor the growth rate of the crystalline layer. As each monolayer is grown the intensity of the reflection beam on the pattern will oscillate. Each oscillation period corresponds to one monolayer of crystal grown (see Fig. 3.3). However, in III-nitrides grown under group-III rich conditions, the intensity of the RHEED pattern does not oscillate enough over time to provide an accurate measure of the growth rate.[6] The experimental set up, that is included in the MBE growth chamber, is presented in Fig. 3.1, while Figure 3.4 shows possible diffraction patterns obtained by RHEED for various types of crystals.

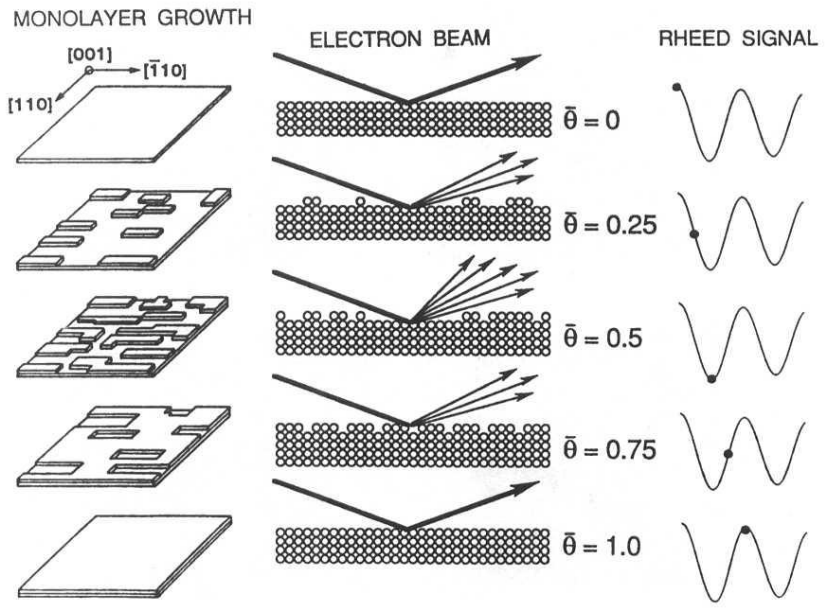

Fig. 3.3. Real space representation of the formation of a single complete monlayer. Θ is the fractional layer coverage. Corresponding RHEED oscillation signal is shown *[Figure taken from Ohring's book "Materials Science of Thin Films", Elsevier Science Publishing Co Inc.].*[7]

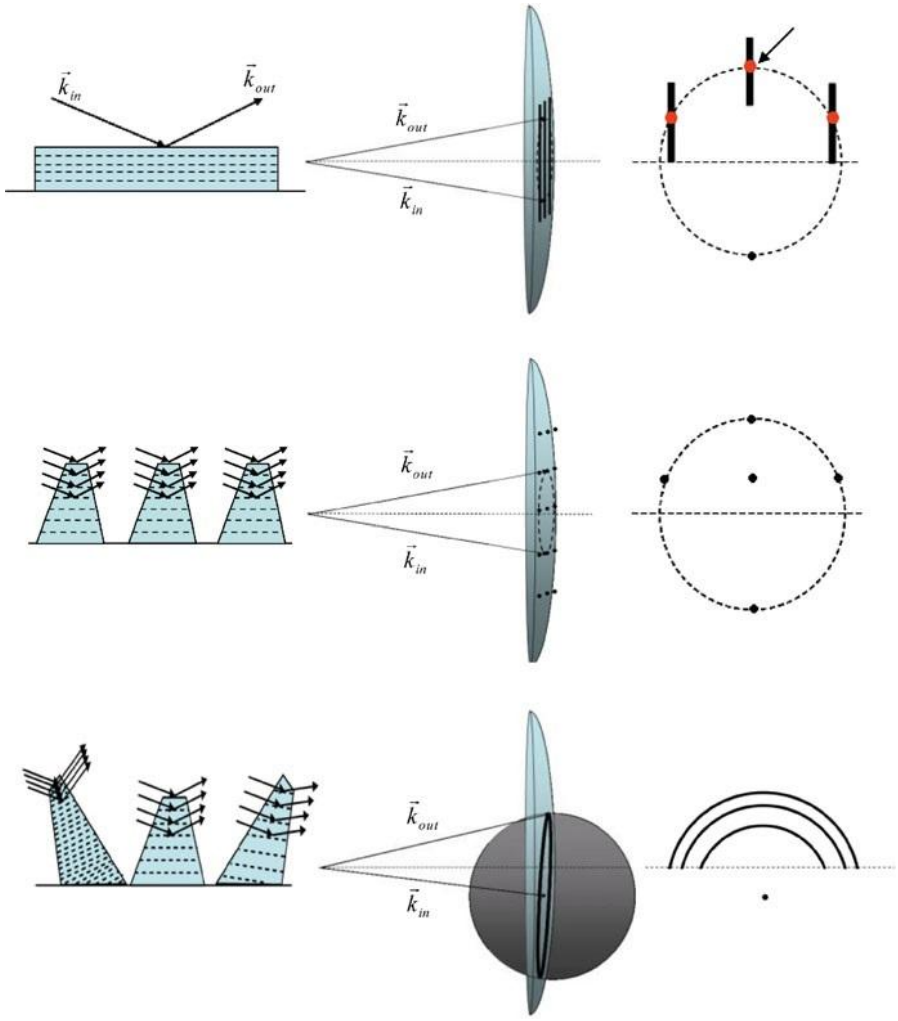

Fig. 3.4. Different diffraction patterns that may be observed by RHEED *[Figure taken from Wang's & Lu's book "RHEED Transmission Mode and Pole Figures", Springer Publishing Company]*.[4] The upper image shows the RHEED pattern for a 2D growth mode of a layer with flat surface (streaky pattern), the image in the middle refers to a 3D growth mode through the formation of 3D islands (spotty pattern), while the image in the bottom corresponds to the growth of a polycrystalline material.

3.2.2 Atomic Force Microscopy (AFM)

AFM is an extremely useful tool for materials characterization that provides the surface morphology of the samples after they are grown. In AFM, a small tip (~30 nm) is placed on a cantilever very close to the sample surface (~1-2 ºA).[8] Atomic attractive forces between the surface and the tip are measured and kept constant by an electronic feedback loop.[8] Therefore the size of the tip is what determines the image analysis. In order to achieve precision movements in all directions, we also use piezoelectric crystals which expand and contract depending on the applied voltage at their edges.

There are different operation modes of an AFM depending on the position of the tip in relation to the surface of the sample (contact mode, tapping mode, non-contact mode). For example, it is possible to trace the surface features without making contact to the surface (non-contact mode), by tracking the movement of the tip with respect to the surface as the atomic forces change. The method we used was the *tapping mode*, where the silicon tip is attached to the end of a cantilever, which oscillates at a constant frequency (near its resonance frequency) on the z axis (perpendicular to the surface of the sample). The amplitude of this oscillation ranges from 20 to 100 nm. As a result, the tip oscillates and it tapes the surface of the sample slightly at the lower point of the oscillation. This method keeps the amplitude of the oscillation constant, hence the mean value of the signal, so the changes, e.g. at the surface of the sample, will give different signals and this will create the final image after the scanning of the whole surface. The main disadvantage of this method may be the lower scanning speed but its main advantages are that we avoid sample scratching, due to the lack of lateral forces and because we have smaller vertical forces between the tip and the sample, as well as the better image analysis.

The microscope that was used, with the valuable help of Katerina Tsagaraki, is a Digital Instruments Nanoscope IIIa operating in tapping mode. The system was mounted on a tripod anti-vibration stage and was capable of lateral resolution of ~10 nm and vertical resolution of ~1 nm.

3.2.3 Resistivity and Hall-Effect measurements

Resistivity and Hall-effect measurements are used in order to determine the carrier concentration and the mobility in semiconductors.[9] By measuring the current (I) that flows through the semiconductor, when a voltage difference (V) is applied at its edges, as it is shown in Fig. 3.5, the resistivity (ρ) is calculated by the relationship:

$$\rho = \frac{wd}{l}\frac{V}{I} \qquad (3.1)$$

where l,d and w are the dimensions of the sample in x,y and z, respectively.

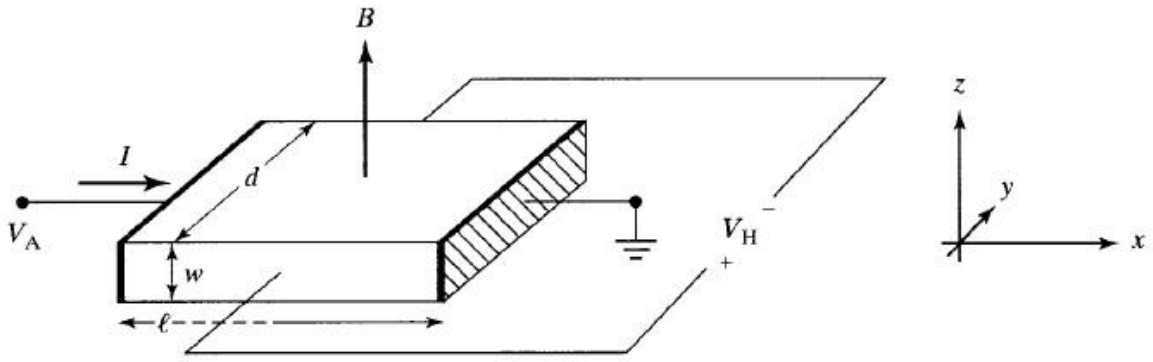

Fig. 3.5. Schematic illustration of the Hall-effect measurement *[Figure taken from Pierret's book "Advanced Semiconductor Fundamentals", Prentice Hall Publications].*[10]

In Hall-effect measurements, the application of a magnetic field (B) perpendicular to the direction of carrier flow in the semiconductor sample is involved. In this case, except from V, a magnetic field B is applied perpendicularly to I, the carriers are subjected to the Lorentz force that is perpendicular to their movement, resulting in a Hall potential difference, V_H, which is perpendicular to I. The Hall potential difference is given by:

$$V_H = -\frac{BI}{|q|dn} \quad (3.2)$$

where n is the majority carrier concentration. From Equation 3.2, and defining Hall coefficient as $R_H=dV_H/BI$, we get for the majority carrier concentration (electrons or holes):

$$n = -\frac{1}{|q|R_H} \quad (3.3) \qquad \text{or} \qquad p = \frac{1}{|q|R_H} \quad (3.4)$$

The Hall mobility of majority carriers, μ_H, is then given by:

$$\mu_H = \frac{1}{\rho|q|n} = \frac{|R_H|}{\rho} \quad (3.5)$$

For the actual measurements of thin semiconductor layers grown on a substrate, the method developed by van der Pauw was used.[11,12] This method includes multiple geometrically symmetrical measurements, in a parallelepiped shape with four ohmic contacts at samples' corners. The measurements were carried out with the valuable help of Adam Adikimenakis.

References

[1] M. A. Herman & H. Sitter, *Molecular Beam Epitaxy – Fundamentals and Current Status*, Springer Series in Materials Science **7**, Chapter 4 (1988)

[2] F. Rinaldi, *Basics of Molecular Beam Epitaxy (MBE)*, University of Ulm, p. 31 (2002)

[3] E. Dimakis, *Physical Mechanisms in Molecular Beam Epitaxy and Properties of InN (0001) Films*, PhD Thesis, University of Crete (2007)

[4] G-C Wang & T-M Lu, *RHEED Transmission Mode and Pole Figures – Thin Film and Nanostructure Texture Analysis*, Springer Publishing Company (2014)

[5] W. Braun, *Applied RHEED – Reflection High-Energy Electron Diffraction During Crystal Growth*, Springer Tracts in Modern Physics **154**, Chapter 2 (1999)

[6] S. M. Seutter, M. H. Xie, W. K. Zhu, L. X. Zheng, H. S. Wu & S. Y. Tong, *Surface Science* **445**, L71 (2000)

[7] M. Ohring, *Materials Science of Thin Films – Deposition & Structure*, Elsevier Science Publishing Co Inc., Second Edition, Chapter 8 (2001)

[8] G. Binnig, C. F. Quate & Ch. Gerber, Atomic Force Microscope, *Phys. Rev. Lett.* **56**, 930 (1986)

[9] E. H. Hall, *Amer. J. Math.* **2** (1879)

[10] R. F. Pierret, *Advanced Semiconductor Fundamentals*, Modular Series on Solid State Devices, Prentice Hall Publications, Second Edition, Chapter 6 (2003)

[11] L. J. van der Pauw, *Philips Research Reports* **13**, 1-9 (1958)

[12] L. J. van der Pauw, *Philips Research Reports* **20**, 220-224 (1958)

Chapter 4

Schrödinger-Poisson Calculations

The study and fabrication of devices, based on heterostructures, need a detailed research of their electronic properties. At the nanometer scale, electronic properties of devices will be increasingly dominated by quantum effects, until at some point these effects become essential for device operation.[1] These properties can be extracted and analyzed by solving self-consistently Schrödinger's and Poisson's equations (SCSP), for the electron wave functions and the electric potential respectively. Both equations are solved dividing real space into discrete variable mesh points and solving the wave function within those discrete spacings.[2] The finite difference method (FDM) is a simple and efficient method for solving ordinary differential equations (ODEs) in problem regions with simple boundaries. We note that in nanostructures the requirement of self-consistency is of great importance, since the carrier densities can vary substantially over the dimensions of the structure. Self-consistency practically means that, the electron concentration produces an electric potential that produces that same electron concentration through solution of the Schrödinger equation, when it is combined with the potential of the structure.

The basic solving idea for the problem is to start with a trial potential $V(z)$ and solve Schrödinger's equation. Having derived the wave functions, we can calculate the electron density distribution $n(z)$ by summing the electron occupation for each state multiplied with the respective probability of an electron being in that state. The calculated $n(z)$ and a given donor

concentration $N_D(z)$ can be used to compute the electrostatic potential $\varphi(z)$ and after that, we can calculate the new potential energy *V(z)*. Finally, we iterate this procedure until convergence. The conduction band (CB) profiles, along the growth direction z, and 2-Dimensional Electron Gas (2DEG) distribution in equilibrium were obtained using a SCSP solver.[2]

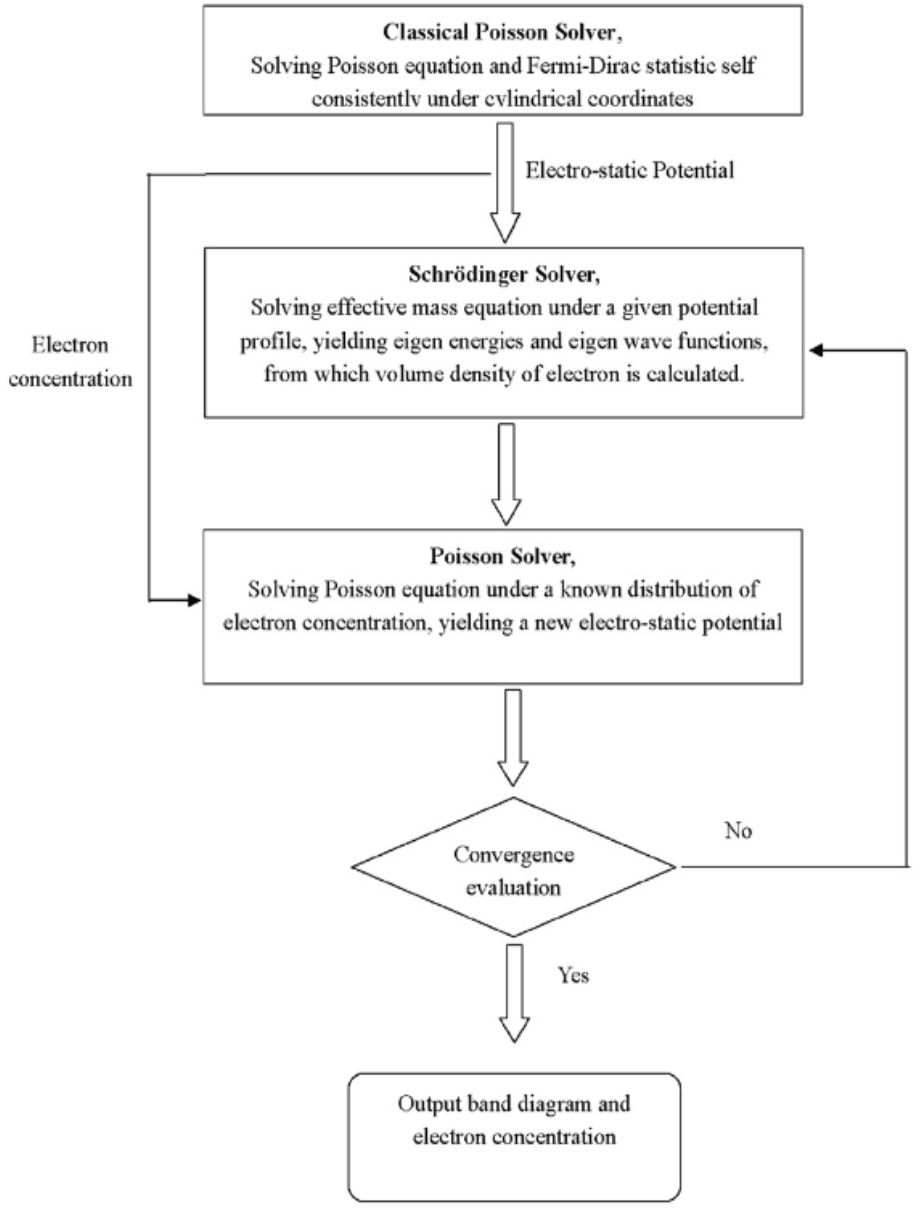

Fig. 4.1. Flow chart of the self-consistent solution of the Schrödinger and Poisson equation *[Figure taken from Wang et al]*.[3]

4.1 Solving the Equations

The one-dimensional *Schrödinger equation* is:

$$-\frac{\hbar^2}{2}\frac{d}{dz}\left(\frac{1}{m^*(z)}\frac{d}{dz}\psi_i(z)\right)+V(z)\psi_i=E_i\psi_i(z) \qquad (4.1)$$

where ψ is the wave function, V is the potential energy, E is the energy, m^* is the effective mass and $\hbar$ is Planck's constant divided by 2π.

The one-dimensional *Poisson equation* gives the idea of charge distribution in the 2DEG and is given by:

$$\frac{d}{dx}\left(\varepsilon_s(z)\frac{d}{dx}\right)\varphi(z)=\frac{-q\left[\sigma_{pol.}/t_{mesh.}+N_D(z)-n(z)\right]}{\varepsilon_0} \qquad (4.2)$$

where ε_s is the dielectric constant, φ is the electrostatic potential, N_D is the ionized donor concentration, $t_{mesh.}$ is the thickness of the discrete mesh points, and n is the electron density distribution.

In the general case, where in a semiconductor we have electrons, holes, ionized donors and ionized acceptors, the charge density (if polarization charges are ignored) is calculated by the equation:

$$\rho=q\left[p(z)+N_D^{+}(z)-n(z)-N_A^{-}(z)\right] \qquad (4.3)$$

In a quantum well, the potential energy V is related to the electrostatic potential φ as follows:

$$V(z) = -q\varphi(z) + \Delta E_c \qquad (4.4)$$

where ΔE_c is the pseudopotential energy due to the band offset at the heterointerface.

The wave function $\psi(z)$ in Eq. (4.1) is related to the electron density $n(x)$ in Eq. (4.2), with the following way:

$$n(x) = \sum_{k=1}^{m} \psi^*{}_k(x)\psi_k(x)n_k \qquad (4.5)$$

where m is the number of bound states and n_k is the electron occupation for each state.

The electron concentration for each state can be found by integrating the density of states function and the Fermi-Dirac probability function:

$$n_k = \frac{m^*}{\pi\hbar^2}\int_{E_k}^{\infty} \frac{1}{1+e^{(E-E_F)/kT}} dE \qquad (4.6)$$

where E_k is the eigenenergy.

4.2 Approximations and Assumptions

At this point we have to mention some key assumptions we used in the calculations, regardless of the type of the structure that was simulated.[2]

- We assumed non-interacting electrons model.
- We assumed that donors and acceptors were fully ionized, regardless of temperature. For GaN we considered $N_D = 10^{16}$ cm^{-3}, for AlN $N_D = 10^{13}$ cm^{-3} and all simulations were made for T = 300 K.
- We considered equilibrium conditions ($E_F = 0$ for each z).
- The possible boundary conditions used in calculations (Ohmic or Schottky contact) were defined as markers on the surface and substrate of the structure. In the case of a Schottky contact, we used a potential barrier height of, $\varphi_b = 1$ eV at GaN surface and $\varphi_b = 3$ eV at AlN surface. In the case of an Ohmic contact, the calculation was done assuming charge neutrality at the edges of the structure.
- The amount of defect-induced charges was ignored in our calculations.
- The induced sheet carrier charges at the top (gate contact) and bottom (GaN/nucleation layer) interfaces, due to the discontinuity in the polarization values, were neglected.
- Surface states were not considered (except from chapter 5.3) but they may be of importance as they act as a source of electrons.

4.3 Material Parameters

The material parameters of ternary alloys, like $Al_xGa_{1-x}N$, are usually calculated by a linear interpolation between the values of the binary compounds (AlN and GaN), known as Vegard's law. Vegard's law is a good approximation for macroscopic quantities, like lattice parameters, but it does not hold so well for microscopic properties, like energy bandgaps[4,5] and polarization (spontaneous and piezoelectric),[6,7] where a nonlinear dependency exists. This is overcome by introducing a so-called *bowing parameter* which leads to a 2nd order polynomial. The nonlinearity found in some alloy properties is due to the internal stress caused by the lattice mismatch of the alloy constituents.[5,7] We used linear and quadratic interpolations to describe the physical properties of the alloys in our calculations. All the relevant parameters, used in the calculations, were according to Ambacher et al.[6] The conduction band discontinuities ΔE_C were according to Van de Walle et al.[8] and the bowing parameters in energy gaps were according to Androulidaki et al.[5]

4.3.1 Lattice Constant

The hexagonal unit cell of the wurtzite structure $Al_xGa_{1-x}N$ has two lattice parameters to which Vegard's law can be applied[7]:

$$a_{AlGaN}(x) = (3.1986 - 0.0891x)\,\mathring{A} \qquad (4.7)$$

$$c_{AlGaN}(x) = (5.2262 - 0.2323x)\,\mathring{A} \qquad (4.8)$$

4.3.2 Energy Bandgap

The band gap energy is perhaps the most important parameter in semiconductor physics and is modeled with both a temperature and a compositional dependence.[7] The compositional dependence of the principal bandgap of $Al_xGa_{1-x}N$ shows a nonlinear increase of the bandgap with increasing Al-content[7]:

$$E_{AlGaN}^{g}(x) = \left[6.28x + 3.42(1-x) - 1.00x(1-x)\right] \text{ eV} \quad (4.9)$$

4.3.3 Dielectric Constant

The relative dielectric constant of the $Al_xGa_{1-x}N$ alloy is a linear interpolation between the dielectric constants of the binary alloys GaN and AlN[7]:

$$\varepsilon_{AlGaN}(x) = (0.03x + 10.28) \quad (4.10)$$

4.3.4 Schottky Barrier Height

We assumed a nickel (Ni) Schottky barrier contact at the $Al_xGa_{1-x}N$ surface, or a similar Fermi level pinning at a bare $Al_xGa_{1-x}N$ surface. The following dependence on x is found to hold[7]:

$$e\phi_{AlGaN}(x) = (2.2x + 0.8) \text{ eV} \quad (4.11)$$

4.3.5 Energy Band Offset

An energy offset is used to align the valence (or the conduction) band of different materials. In this work GaN is chosen as the reference for the III-V materials. The energies of the conduction band edges are calculated by[8]:

$$\Delta E^{C}_{AlGaN}(x) = 0.7\left(E^{g}_{AlGaN}(x) - E^{g}_{GaN}\right) \qquad (4.12)$$

4.3.6 Polarization

Spontaneous Polarization

Because of the non-linear dependence of the cell-internal parameter u on alloy composition,[7] and the significant contribution of different cation electronegativities,[9] a non-linear behavior of the spontaneous polarization versus x has to be expected for ternary alloys.[7] As we can see below, the first two terms in the equations are the usual linear interpolation, between the binary compounds (AlN and GaN), and the third term is embodying non-linearity to quadratic order:

$$P^{SP}_{AlGaN}(x) = \left[-0.090x - 0.034(1-x) + 0.021x(1-x)\right]\ C/m^2 \qquad (4.13)$$

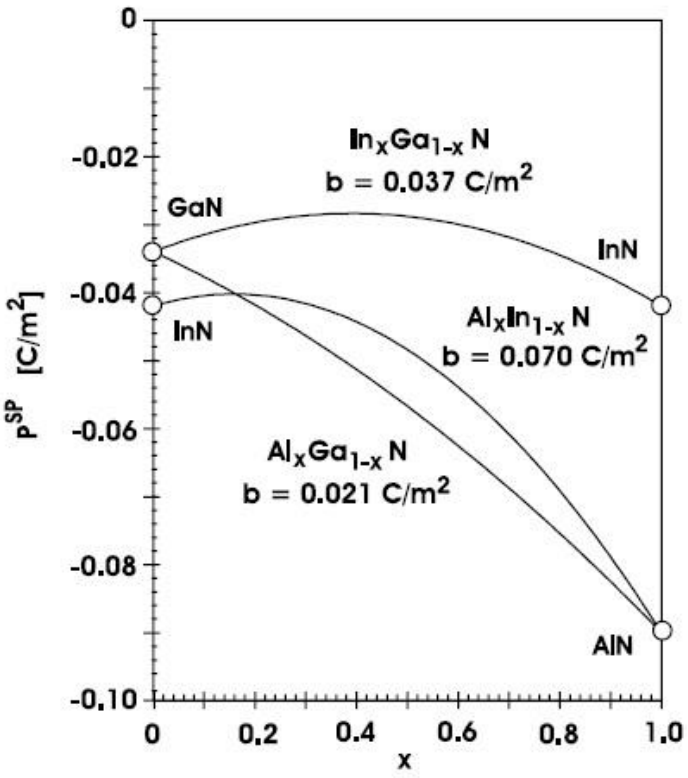

Fig. 4.2. Predicted spontaneous polarization for random ternary III-Nitride alloys with wurtzite crystal structure *[Figure taken from Bernardini & Fiorentini]*.[9]

Piezoelectric Polarization

The non-linear dependence of the piezoelectric polarization on the $Al_xGa_{1-x}N$ alloy composition can be approximated with an accuracy of better than 1% by the following quadratic equations[7], for the cases of fully strained AlGaN on relaxed buffer layers of GaN and AlN:

$$P_{AlGaN/GaN}^{PZ}(x)=\left[-0.0525x+0.0282x(1-x)\right]\ C/m^2 \qquad (4.14)$$

$$P_{AlGaN/AlN}^{PZ}(x)=\left[0.026(1-x)+0.0248x(1-x)\right]\ C/m^2 \qquad (4.15)$$

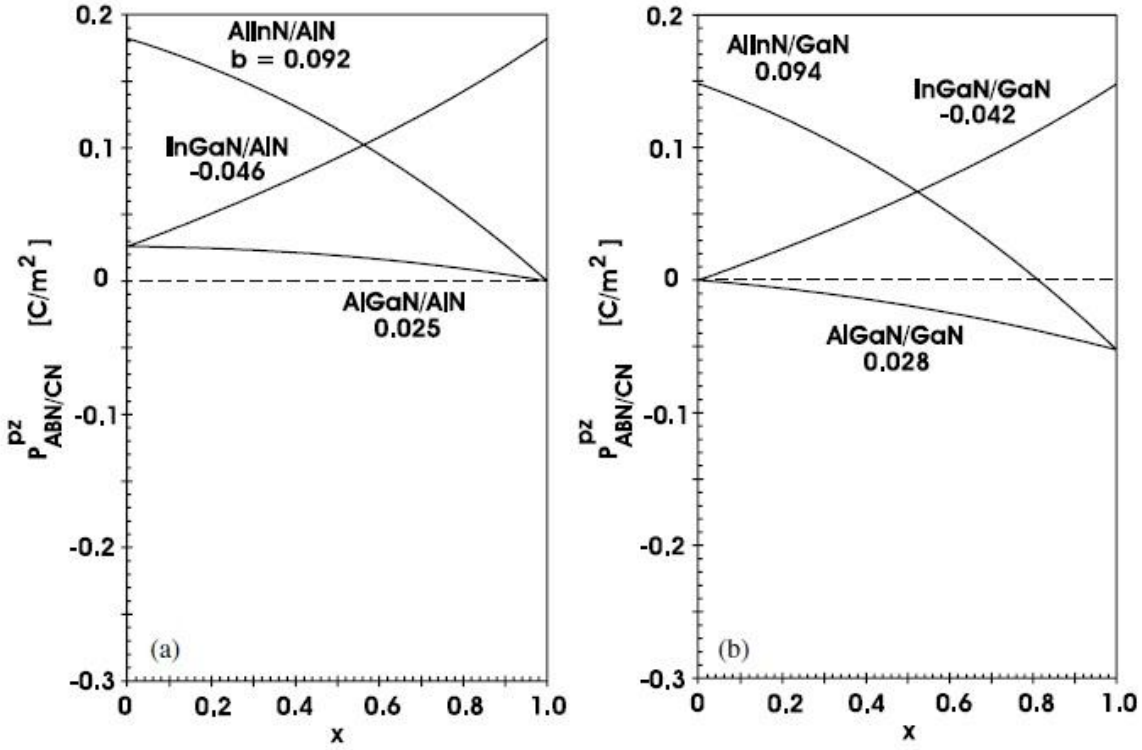

Fig. 4.3. The piezoelectric polarization of ternary III-Nitride alloys pseudomorphically grown on relaxed (a) AlN buffer layers and (b) GaN buffer layers *[Figure taken from Bernardini & Fiorentini].*[9]

References

[1] A. Trellakis, A. T. Galick, A. Pacelli & U. Ravaioli, *J. Appl. Phys.* **81** (12), 7880 (1997)

[2] I-H. Tan, G. L. Snider, L. D. Chang & E. L. Hu, *J. Appl. Phys.* **68** (8), 4071-4076 (1990)

[3] L. Wang, D. Wang & P. M. Asbeck, *Solid-State Electronics* **50**, 1732-1739 (2006)

[4] J. Piprek, *Nitride Semiconductor Devices: Principles and Simulation*, Wiley-VCH Verlag (2007)

[5] M. Androulidaki, N. T. Pelekanos, K. Tsagaraki, E. Dimakis, E. Iliopoulos, A. Adikimenakis, E. Bellet-Amalric, D. Jalabert & A. Georgakilas, *Phys. Status Solidi C* **3**, 1866 (2006)

[6] O. Ambacher et. al., *J. Phys.: Condens. Matter* **14**, 3399-3434 (2002)

[7] C. Wood & D. Jena, *Polarization Effects in Semiconductors – From Ab Initio Theory to Device Applications*, Eds. C. Wood & D. Jena, Springer Publications (2008)

[8] C. G. Van de Walle & J. Neugebauer, *Nature* **423**, 626-628 (2003)

[9] F. Bernardini & V. Fiorentini, *Phys. Rev. B* **64**, 85207 (2001)

Chapter 5

Results & Discussion

5.1 Optimization of single AlN/GaN HEMT heterostructure

5.1.1 Theoretical Calculations

Simple AlN/GaN heterostructures were studied, with a single thin AlN barrier (1.5 - 4.5 nm) developed epitaxially on a 1-μm-thick and Ga-polarity GaN (0001) layer. The aim of this study was the physical understanding of such heterostructures and the prediction of the 2-Dimensional Electron Gas (2DEG) properties that is created at the AlN/GaN interface due to differences in polarizations. These properties make such heterostructures suitable applicants for the fabrication of High Electron Mobility Transistors (HEMTs). A self-consistent Schrödinger-Poisson (SCSP) solver[1] was employed to determine the equilibrium energy band profiles and 2DEG density of the HEMT structures and the effects of AlN barrier and GaN cap layer thicknesses. All relevant parameters, used in the calculations, were according to Ambacher et al.[2] and the conduction band discontinuities ΔE_C were according to Van de Walle et al.[3] For the boundary conditions, the energy distance $(E_C\text{-}E_F)_S$ between conduction band E_C and Fermi level (E_F) at the GaN surface was set at 1 eV, while neutrality was considered at the bottom (GaN) side. For donor concentrations, we assumed $N_D = 10^{16}$ cm^{-3} for GaN and $N_D = 10^{13}$ cm^{-3} for AlN.

Effect of GaN cap layer

Initially, the effect of GaN coating (cap) layer on the AlN barrier layer was studied by varying the thickness of the GaN cap from 1 to 10 nm. We noticed that, the thicker the GaN cap layer on the surface is, the lower the surface charge 2DEG density (N_S) we get. Typically, the study of the 1 nm GaN/4.5 nm AlN/300 nm GaN structure gave $N_S = 2.7x10^{13}$ cm^{-2}, while for the 10nm GaN/4.5 nm AlN/300 nm GaN structure we obtained $N_S = 5.5x10^{12}$ cm^{-2}. This reduction in the concentration of 2DEG was expected and is physically explicable. When depositing a thin GaN layer over the layer of AlN barrier, a surface negative polarization charge is generated at the upper GaN/AlN interface, which equals to the positive polarization charge of the lower AlN/GaN interface and leads to a decrease of the 2DEG density formed at the lower interface. The effect of the opposite polarization charge at the upper GaN/AlN interface becomes more intense as the thickness of the GaN cap layer increases (see Fig. 5.1).

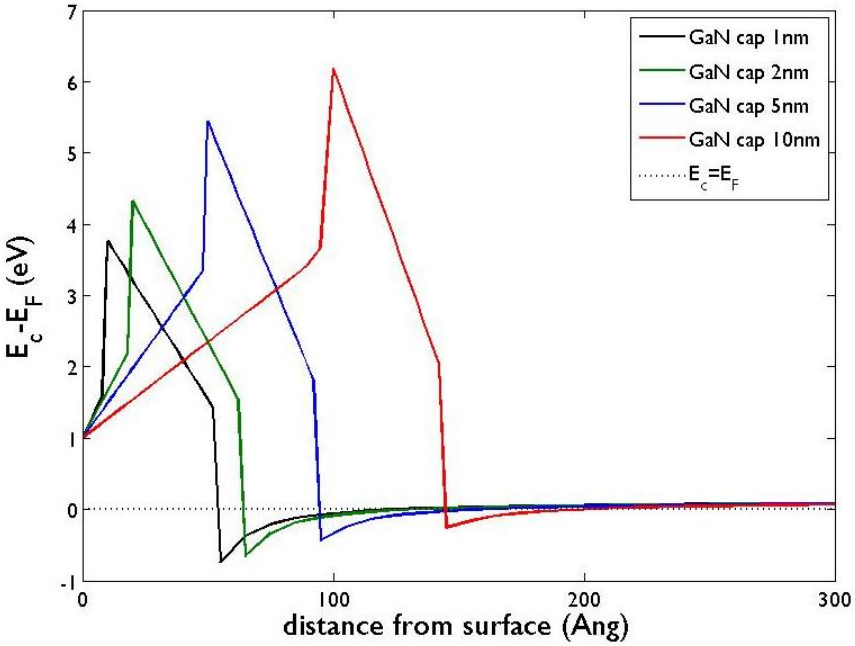

Fig. 5.1. Simulated conduction band diagrams for [t (nm) GaN/4.5 nm AlN/300 nm GaN] structures, where t = 1, or 2, or 5, or 10 nm.

Figure 5.1 shows the distributions of the conduction bands as a function of distance from the surface, for heterostructures with different GaN cap thicknesses. We notice that, as the GaN thickness increases, the depth of the well, created at the lower AlN/GaN interface, is reduced. It should be noted that the SCSP calculations, for the structure at the equilibrium, predict that a large GaN cap thickness may also result to accumulation of holes within the AlN layer, at its top interface (EV will approach EF). However, this could not be realized due to the n-type background doping of the layers and the negligible intrinsic carrier concentration in wide bandgap materials.

The calculated values of 2DEG density are plotted, as a function of the GaN cap thickness, in the diagram shown in Figure 5.2. The decreasing dependence of 2DEG density on the GaN cap layer thickness is presented.

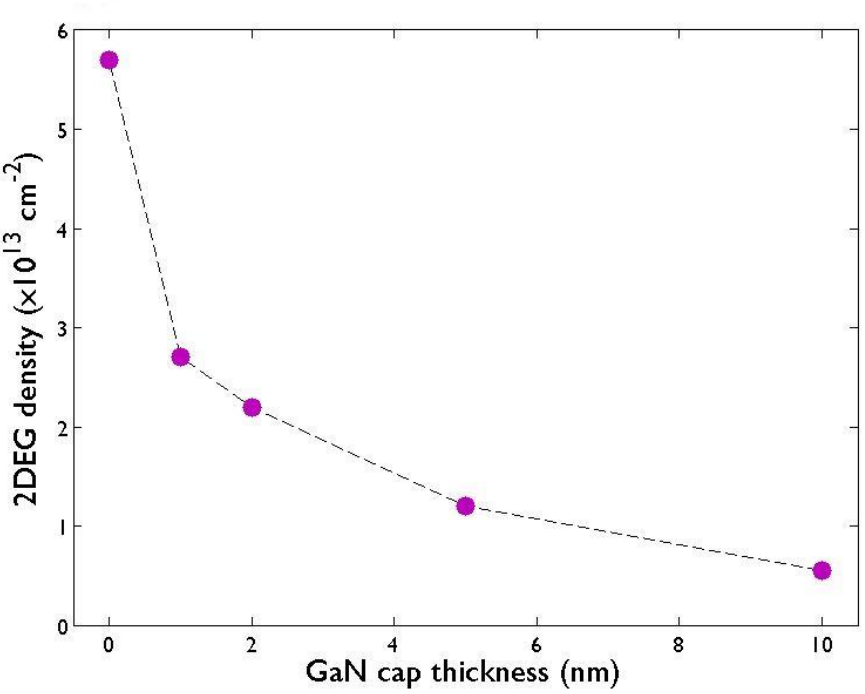

Fig.5.2. Theoretical 2DEG density as a function of GaN cap thickness for [t (nm) GaN/4.5 nm AlN/300 nm GaN] structures, where t = 0, or 1, or 2, or 5, or 10 nm.

Effect of AlN barrier thickness

After we reached the conclusion that the GaN cap on the surface should be as thin as possible, structures with 1 nm GaN cap were studied. In particular, 1 nm GaN/t_b (nm) AlN/300 nm GaN structures were studied for the effect of AlN layer thickness for values in the range of 1.5 nm to 4.5 nm. The results of the calculations showed that the thicker the AlN layer is, the higher the values we get for the 2DEG sheet density. Specifically, for 4.5 nm AlN we obtained an electron sheet density Ns = 3.1×10^{13} cm^{-2}, while for 1.5 nm AlN the respective value was N_S = 3.8×10^{12} cm^{-2}. However, there are experimental limitations on the maximum permissible thickness of AlN barrier due to the large difference in the lattice constants of the two materials. The relaxation of the misfit strain of the AlN layer results to dislocations and microcracks in the AlN layer. It has been determined that the maximum allowable thickness is 5nm for AlN grown on GaN (0001).[4]

Some basic diagrams, resulted from the self-consistent solving of the Schrödinger-Poisson equations in the direction of the heterostructures formation, are presented below. The two extreme cases that were examined, concern structures with 1.5 nm and 4.5 nm AlN. Figure 5.3 shows the variation of the conduction band as a function of the distance from surface, for all different AlN thicknesses, while Figure 5.4 shows the dependence of 2DEG density on the AlN barrier thickness. As we have already mentioned, the thicker the AlN layer is, the higher the values we get for the surface density of electrons due to the deepening of the quantum well which is created in the interface of the two materials.

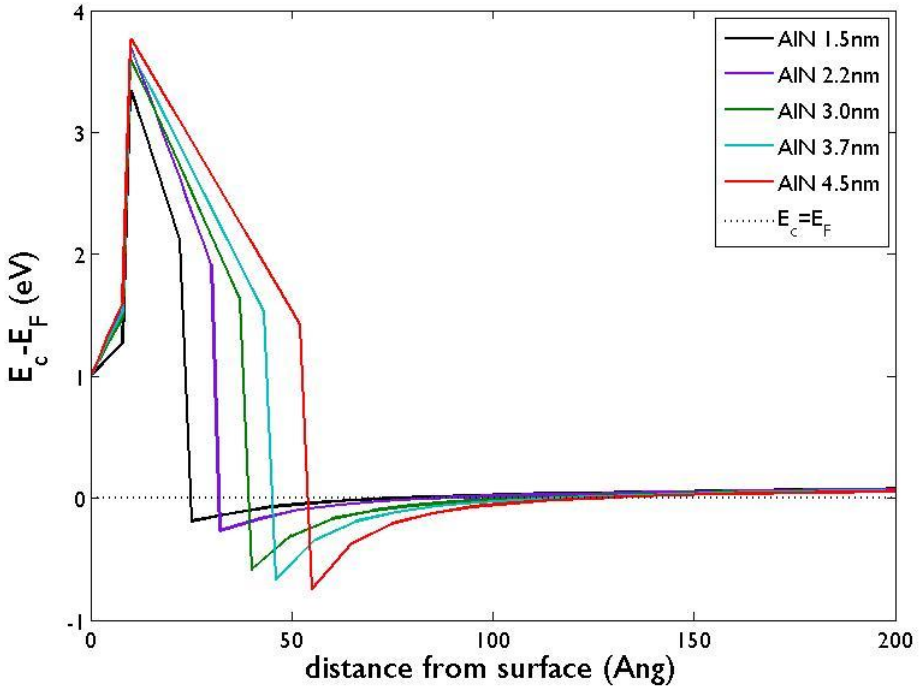

Fig. 5.3. Simulated conduction band diagrams for [1 nm GaN/ t_b (nm) AlN/ 300 nm GaN] structures, where t_b = 1.5, or 2.2, or 3.0, or 3.7, or 4.5 nm.

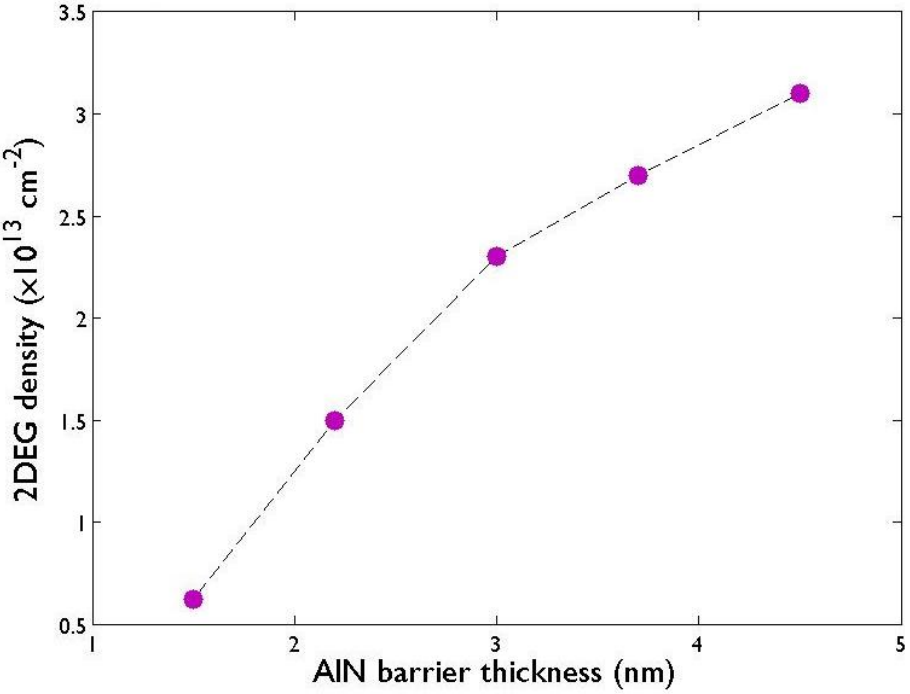

Fig. 5.4. Theoretical 2DEG density as a function of AlN barrier thickness for [1 nm GaN/ t_b (nm) AlN/ 300 nm GaN] structures, where t_b = 1.5, or 2.2, or 3.0, or 3.7, or 4.5 nm.

5.1.2 Epitaxial Growth and Characterization

The simple heterostructure AlN/GaN HEMT consists of a thin layer of AlN barrier, developed on a thick GaN (0001). To study its features, it was deemed necessary initially to optimize the epitaxial growth parameters, in order to achieve high carrier mobility within the HEMT channel. The influence of the AlN layer thickness on the electric properties of the heterostructures (mobility and 2DEG density) was then studied and transistors with a gate length of 1 μm were fabricated and characterized.

The epitaxial growth of AlN/GaN heterostructures was performed using a plasma-assisted MBE system (see Fig. 3.1). Commercially available 3-μm-thick Ga-polar GaN substrates, grown on sapphire (0001) using the MOCVD technique, were used. This ensures the repeatability of the results, the good uniformity and the good crystal quality, while it also saves time. The growth process is as follows: initially the substrates are heated to 700 ° C in ultra-high vacuum conditions, to clean the surface from any adsorbed species, and then a 1-μm-thick GaN layer under Ga-rich conditions is grown. Then the AlN barrier layer is grown, with the presence of a Ga-flux surfactant, and finally a very thin GaN cap layer (usually 1 nm) is grown to protect the AlN layer from oxidation.

Growth optimization of GaN was aimed in order to achieve the optimal possible crystal quality, purity of the material and atomically smooth surface, which are essential factors for the HEMT type transistor technology. For this purpose, GaN was grown in Ga-rich conditions and the RHEED technique was used in order to control the concentration of Ga adatoms on the surface during the growth. Material with good crystal quality and atomically smooth surfaces was obtained, as shown in Figure 5.5.

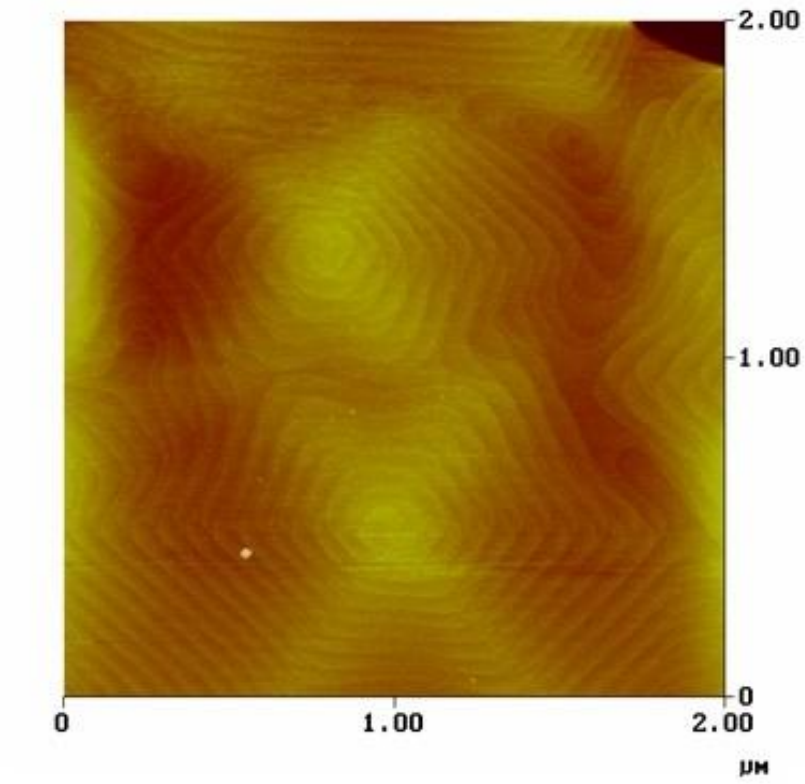

Fig. 5.5. AFM micrograph (2x2 µm) showing the surface of a GaN layer grown by PAMBE on a (0001) GaN/Al_2O_3 substrate.

HEMT structures with different AlN barrier layer thicknesses were then grown and their electrical properties (electron concentration and electron mobility) were measured by Hall-effect measurements. These measurements were made in square-shaped pieces (approximately 5x5 mm) using 4 indium contacts. All samples were grown on same substrates and under similar growth conditions. Figure 5.6 (a) shows the aggregate results for N_S, while Fig. 5.6 (b) shows electron mobility dependence on the AlN barrier thickness.

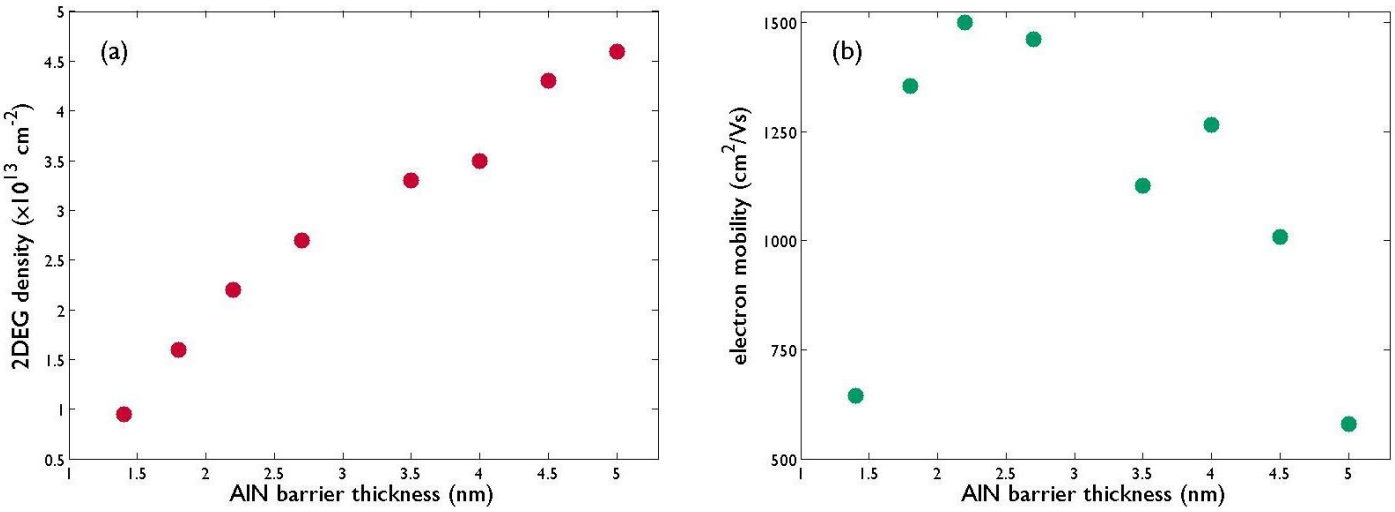

Fig. 5.6. (a) Experimental 2DEG density and (b) electron mobility, both obtained by Hall-effect measurements, as functions of AlN barrier thickness for [1 nm GaN/ t_b (nm) AlN/ 300 nm GaN] structures, where t_b = 1.4, or 1.8, or 2.2, or 2.7, or 3.5, or 4.0, or 4.5, or 5.0 nm.

As we can see, N_S increases almost linearly with AlN barrier thickness and reaches very high values, up to 4.6 x 10^{13}cm^{-3}. At the same time, electron mobility is reduced from 1500 cm^2/Vs (for AlN 2.2 nm) to ~1000 cm^2/Vs for a maximum AlN thickness of 4.5 nm. For higher AlN thicknesses, mobility decreases sharply, due to the formation of micro-cracks, as was observed by SEM scan images. Such a case is shown in Fig. 5.7, where the formation of a micro-crack is clearly distinguishable in a 5-nm-thick AlN layer. Therefore, we can conclude that the *critical thickness* of AlN for avoiding micro-cracking is 4.5 nm. Finally, we notice that for AlN thicknesses less than 2 nm the mobility is significantly reduced and this may due to the increased carrier scattering which arises from reduced electron screening.

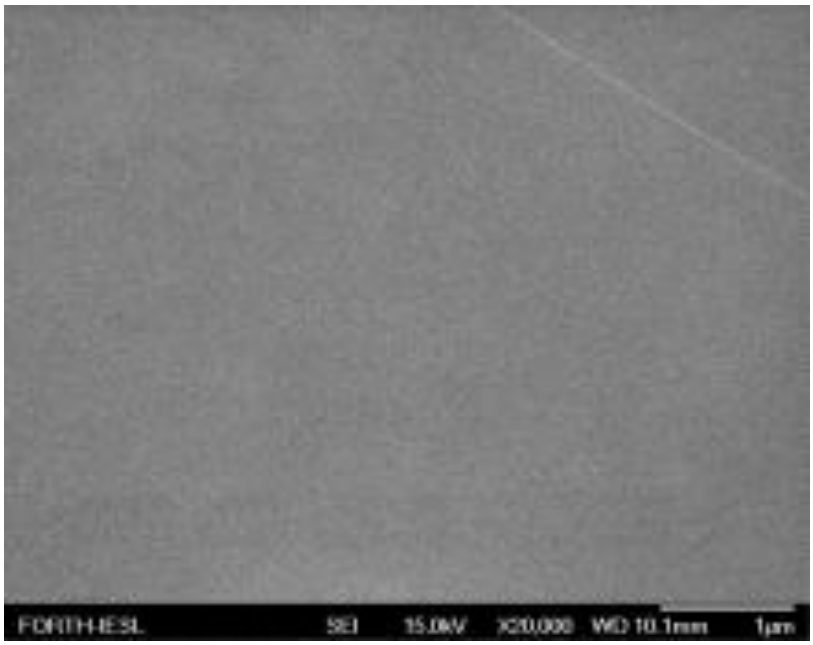

Fig. 5.7. SEM micrograph showing the formation of a micro-crack in a 5-nm-thick AlN layer.

Hall-effect measurements were also carried out at a temperature of 77 K (liquid nitrogen temperature) and the results are summarized in Table 1. We observe that, at 77 K there is a negligible reduction of the electron density, while the electron mobility increases significantly, which proves that measured carrier concentrations are due to the 2DEG. Especially in the case of thin AlN layers (1.8-2.7 nm), the mobility increases almost by a factor of 5.

	AlN thickness	1.4 nm	1.8 nm	2.2 nm	2.7 nm	3.5 nm	4.0 nm	4.5 nm
RT	R (Ω/sq)	1025	286	192	158	167	151	144
	N_S (cm^{-2})	$9.5x10^{12}$	$1.6x10^{13}$	$2.2x10^{13}$	$2.7x10^{13}$	$3.3x10^{13}$	$3.5x10^{13}$	$4.3x10^{13}$
	μ_H (cm^2/Vs)	645	1355	1500	1461	1126	1265	1009
77 K	R (Ω/sq)	240	68	46	43	63	59	105
	N_S (cm^{-2})	$8.1x10^{12}$	$1.4x10^{12}$	$1.8x10^{13}$	$2.4x10^{13}$	$2.9x10^{13}$	$3.2x10^{13}$	$4.1x10^{13}$
	μ_H (cm^2/Vs)	3197	6669	7325	6038	3424	3335	1455

Table 5.1. Hall-effect measurements, for single AlN/GaN HEMT heterostructures, carried out at room temperature and at liquid nitrogen temperature (77 K). The heterostructures consist of [1 nm GaN/ t_b (nm) AlN/ 300 nm GaN] structures, where t_b = 1.4, or 1.8, or 2.2, or 2.7, or 3.5, or 4.0, or 4.5, or 5.0 nm.

References

[1] I-H. Tan, G. L. Snider, L. D. Chang & E. L. Hu, *J. Appl. Phys.* **68** (8), 4071-4076 (1990)

[2] O. Ambacher et. al., *J. Phys.: Condens. Matter* **14**, 3399-3434 (2002)

[3] C. G. Van de Walle & J. Neugebauer, *Nature* **423**, 626-628 (2003)

[4] A. Adikimenakis, *Molecular Beam Epitaxy of (In)AlN/GaN Heterostructures for High Electron Mobility Transistors*, PhD Thesis, University of Crete (2009)

[5] M. Zervos, A. Kostopoulos, G. Constantinidis, M. Kayambaki & A. Georgakilas, *J. Appl. Phys.* **91** (7), 4387-4393 (2002)

[6] Y. Zhang & J. Singh, *J. Appl. Phys.* **85** (1), 587-594 (1999)

5.2 Electron density and currents of double heterostructure AlN/GaN HEMTs[1,2]

The AlN/GaN heterojunction offers the highest polarization discontinuity for GaN two-dimensional electron gas (2DEG) channel transistors and HEMT devices can be realized with ultra-shallow channels and very high current density.[3-5]

The GaN HEMTs are based on heteroepitaxial material and, typically, a 3-4 μm thick GaN buffer layer is initially grown. However, electrons at high drain bias can spill over into the buffer, increasing low frequency noise and resulting in a decreased transconductance[6] and off-state leakage. Current collapse has been also attributed to GaN buffer traps.[7] The GaN buffer breakdown field is also inferior to that of an insulating substrate, such as sapphire (Al_2O_3).

Several groups have adopted AlGaN or AlN buffer (or back barrier) layers to increase electron confinement and suppress short-channel effects.[8-10] Similar considerations have motivated the exploration of very thin GaN or GaN/AlN buffer layers.[11-15] The early work of Wu et al[11] demonstrated the increase of breakdown voltage up to 340 V for AlGaN/GaN HEMTs, by reducing, to 0.4 μm, the thickness of the GaN buffer layer on sapphire substrate. The reduced buffer layer thickness is particularly important for sensor applications, considering fabrication, performance and integration issues.[12] The capabilities of double barrier AlN/GaN HEMT structures, with strained GaN quantum well (QW) channel, on AlN substrates have been also demonstrated recently.[9,15]

Due to polarization, a double barrier GaN HEMT structure does not provide simply a back barrier for improved electron confinement but interferes with the formation of 2DEG.[16] The

opposite polarization charge at the bottom GaN/AlN heterojunction (and the created field) will remove electrons from the 2DEG induced underneath the top AlN/GaN heterojuction. The high density of threading dislocations in thin heteroepitaxial layers may be responsible for current reduction, due to increased carrier compensation and scattering during transport.

This work aimed to provide physical insight for double barrier AlN/GaN HEMT structures, consisting of an AlN barrier (with 1 nm GaN cap) on a thin GaN/AlN buffer layer. The case of a relaxed GaN thin buffer layer on a thin AlN buffer-nucleation layer was considered. The double barrier HEMT structures were analyzed both theoretically and experimentally and the effects of (a) AlN (top) barrier thickness and (b) GaN buffer thickness, on the 2DEG density and transport properties.

5.2.1 Experimental Details and Calculations

Five metal-polarity AlN/GaN HEMT structures, with a thin 300 nm GaN/200 nm AlN buffer layer, were grown heteroepitaxially on insulating Al_2O_3 (0001) substrates by plasma-assisted molecular beam epitaxy (PAMBE).[17,18] The HEMT structures comprised (from top to bottom) 1 nm GaN cap/ t_b (nm) AlN barrier/300 nm GaN buffer/200 nm AlN buffer-nucleation layer, with the AlN barrier thickness t_b being 1.5, or 2.2, or 3.0, or 3.7, or 4.5 nm (see Fig. 5.8). The substrate preparation and nitridation conditions were according to the optimum conditions determined in other works.[16,18] The growth of the 200 nm AlN nucleation-buffer layer on sapphire was carefully optimized, to provide a smooth surface for the overgrown layers.

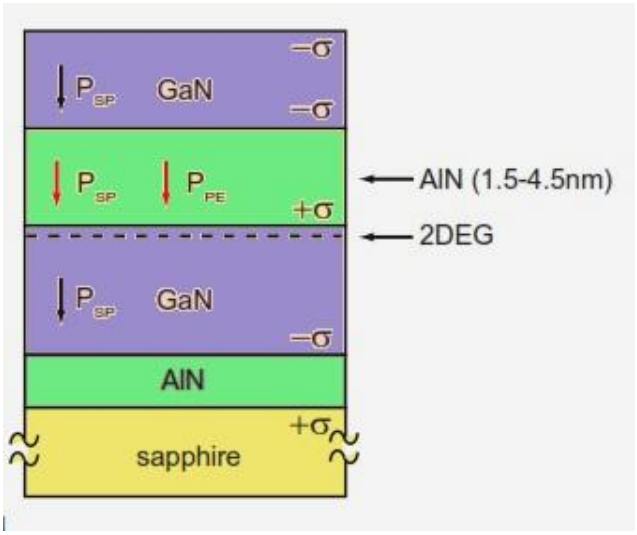

Fig. 5.8. The AlN HEMT structures that have been studied.

Unpassivated HEMT devices, with gate width of $W_g = 50$ μm and gate length $L_g = 1$ μm, as well as Schottky diodes and Hall-effect test patterns were processed by Ch. Zervos.[1,2] The surface morphology of the samples was examined by Atomic Force Microscopy (AFM) and Field Emission Scanning Electron Microscopy (FE-SEM). The 2DEG properties were investigated by Hall-effect measurements at 300 K with a magnetic field of 0.4 T, as well as capacitance versus voltage (C-V) measurements at 1 MHz on Schottky diodes (*measurements carried out by Ch. Zervos*). A self-consistent Schrödinger-Poisson (SCSP) solver[19] was employed to determine the equilibrium energy band profiles and carrier distributions of the HEMT structures and the effects of AlN barrier and GaN buffer thicknesses. All relevant parameters, used in the calculations, were according to Ambacher et al.[20] and the conduction band discontinuities ΔE_C were according to Van de Walle et al.[21] For the boundary conditions, the energy distance $(E_C\text{-}E_F)_S$ between conduction band E_C and Fermi level (E_F) at the GaN surface was set at 1 eV, while neutrality was considered at the bottom (AlN) side. For donor concentrations, we assumed $N_D=10^{16}$ cm^{-3} for GaN and $N_D=10^{13}$ cm^{-3} for AlN.

5.2.2 Results and Discussion

Fig. 5.9[1] is an AFM micrograph showing the surface morphology of an optimized 200 nm AlN nucleation layer, grown on sapphire (0001) substrate by PAMBE. The atomic height steps on the surface indicate AlN growth under a step-flow growth mode, resulting in a very smooth surface with a root-mean-square (rms) roughness of 0.3 nm for a 5 x 5 μm scan. A very smooth AlN nucleation layer surface is very critical for the overgrowth of a thin HEMT structure with low roughness at the AlN/GaN 2DEG interface.[14]

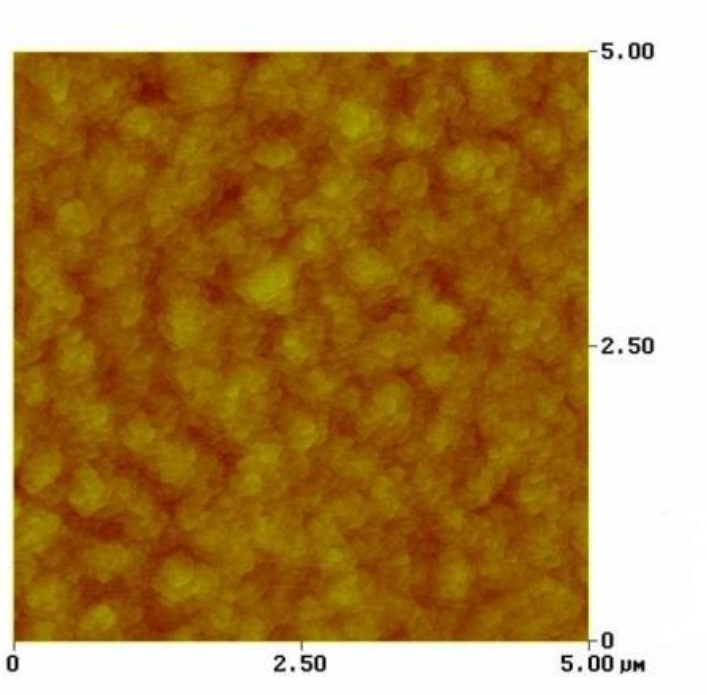

Fig. 5.9. AFM micrograph showing the surface of a 200 nm AlN layer grown by PAMBE on (0001) sapphire substrate. The z-axis range is 2.6 nm.[1]

Figure 5.10 (a)[1] shows the calculated equilibrium band diagram for the HEMT structure with t_b= 4.5 nm. The main plot gives an expanded view of the top region of the structure, where the 2DEG confining QW is formed, whilst the inset shows the band profile for the entire HEMT

structure (from the surface of the 1 nm GaN cap to the bottom side of the AlN nucleation layer). The bottom GaN/AlN interface induces a strong electric field within the thin 300 nm GaN buffer layer and a large barrier for electron motion toward the substrate. However, the calculated 2DEG density, N_S, of 2.1×10^{13} cm^{-3} for the present HEMT structure, with thin GaN/AlN buffer layer, is significantly lower compared to $N_S = 3.1 \times 10^{13}$ cm^{-3} calculated for the same HEMT structure (t_b= 4.5 nm) on a pure GaN buffer layer. The strong electric field in the GaN buffer and the reduction of N_S is due to the negative static polarization charge at the bottom GaN/AlN interface, which is very close to the top AlN/GaN heterojunction where the 2DEG is formed. Further analysis of the effect of the GaN-on-AlN buffer layer thickness on N_S will be presented later.

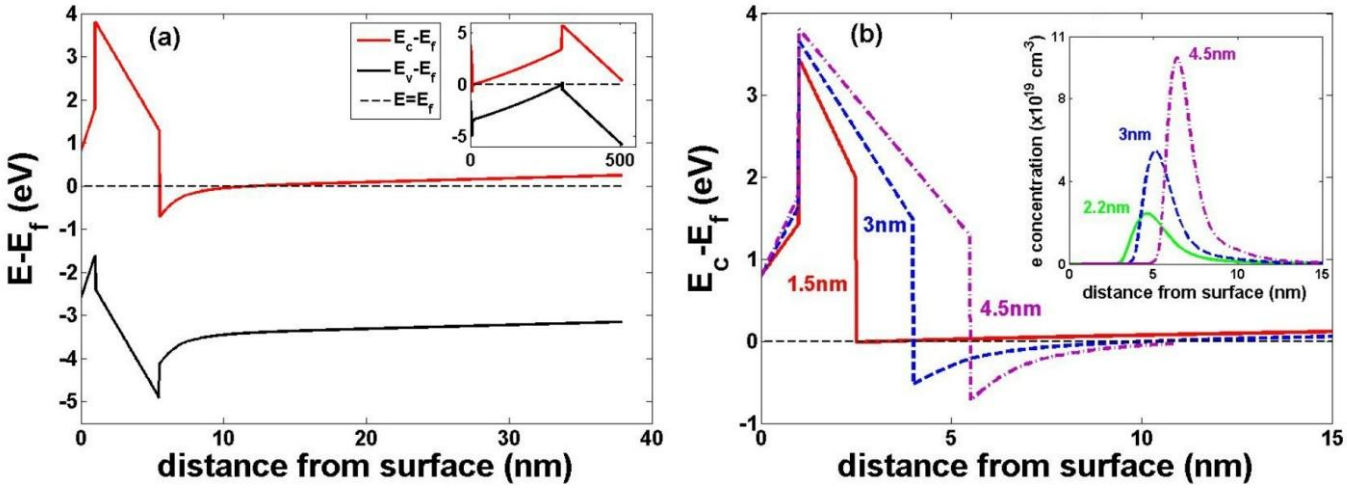

Fig. 5.10. (a) Simulated band diagram for the top region of the structure [1nm GaN/ 4.5 nm AlN/ 300 nm GaN/ 200 nm AlN]. The insert diagram presents the band profile for the entire structure. (b) Simulated band diagrams for [1nm GaN/ t_b(nm) AlN/ 300 nm GaN/ 200 nm AlN] structures, where t_b=1.5, or 3.0, or 4.5 nm. The inset shows the electron distribution for t_b= 2.2, or 3.0, or 4.5 nm.[1]

For the given 300 nm GaN/200 nm AlN buffer layer, the N_S can be modified by changing the HEMT AlN barrier thickness t_b. The calculated conduction band (E_C) profile for the top region of the structure, where the 2DEG forms, is shown in Fig. 5.10 (b)[1] for three different values of t_b (1.5, 3.0 and 4.5 nm). The electron concentration profiles for the t_b values of 2.2, 3.0 and 4.5 nm are shown in the inset of Fig. 5.10 (b)[1]. For t_b= 1.5 nm there is no 2DEG QW formation due to the charge depletion effect of the surface potential. The increase of the AlN thickness, t_b, reduces the built-in electric field within the AlN barrier and deepens the 2DEG QW, with corresponding increase of N_S.

The calculated N_S values are plotted versus t_b, together with the experimental Hall-effect and C-V results, in Fig. 5.11[1]. The N_S values were extracted from C-V measurements by integrating the electron concentration for diode bias from the negative threshold voltage (V_T) that pinches-off the 2DEG up to 0 V.

The theoretical and experimental N_S values are in a very good agreement, suggesting a negligible influence of the crystalline defects that increase near the heteropitaxial interface. The highest, experimentally determined, N_S for the HEMT structure with t_b= 4.5 nm was 2.2×10^{13} cm^{-2} from Hall-effect measurements and 2.0×10^{13} cm^{-2} from C-V measurements, whilst SCSP calculation resulted to 2.1×10^{13} cm^{-2}. The electron mobility increases rapidly for AlN barrier thickness above t_b= 2.2 nm, with the maximum value among the different samples being 900 cm^2/Vs for t_b= 3.0 nm. A small reduction was observed for higher AlN barrier thicknesses, reaching the value of 703 cm^2/Vs for 4.5 nm AlN. This could be attributed to an increase in the interface roughness scattering as the charge distribution shifts closer to the heterointerface at high carrier concentrations.[22] According to our calculations, as shown in the inset of Fig. 5.10 (b)[1], the distance of the peak 2DEG concentration from the top AlN/GaN interface is 1.4, 1.1, 1.0, and 0.9 nm for t_b equal to 2.2, 3.0, 3.7 and 4.5 nm, respectively.

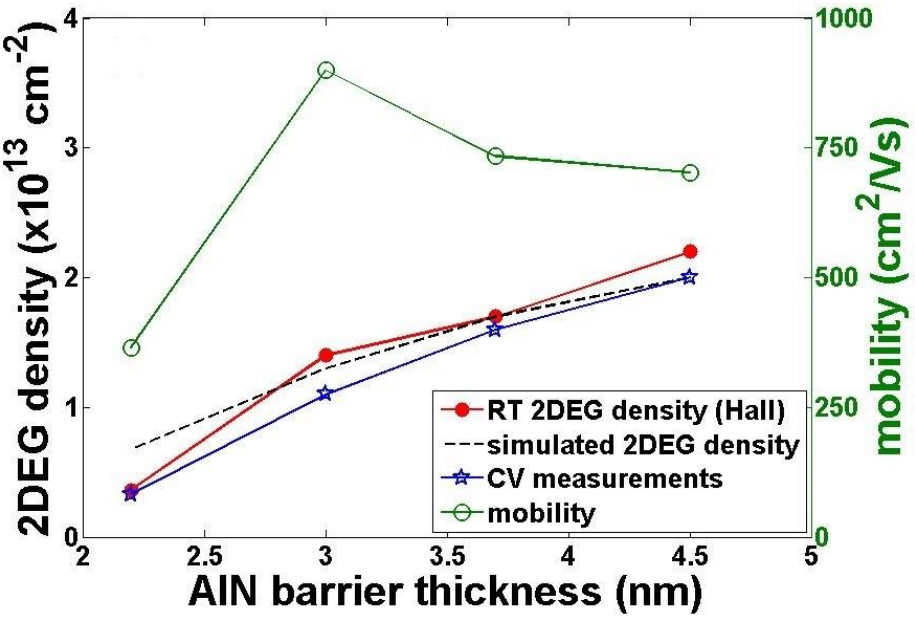

Fig. 5.11. Theoretical (dashed line) and experimental 2DEG density (solid circles for Hall-effect and star-like for C-V measurements), and electron mobility (open circles), as functions of AlN barrier thickness (t_b).[1]

As discussed earlier in the text and is shown in the inset of Fig. 5.10 (a)[1], the bottom GaN/AlN interface has a significant impact on the band profile and 2DEG density of the HEMT structure. To identify the role of the thickness of the GaN buffer layer, a systematic series of SCSP calculations was carried out for HEMT structures consisting of 1nm GaN/ t_b (nm) AlN/ t_{GaN} (nm) GaN/ 200 nm AlN, where the GaN thickness (t_{GaN}) was varied from 25 nm to 10 μm for t_b between 2.2 and 4.5 nm. The calculated N_S values have been plotted versus AlN barrier thickness (t_b) and GaN thickness (t_{GaN}) in Fig. 5.12 (a)[1] and 5.12 (b)[1], respectively. For each t_b value, the N_S increases with increasing t_{GaN} from 25 nm to 10 μm and becomes N_S= 3.0x10^{13} cm^{-2} for t_{GaN}=10 μm and t_b= 4.5 nm, which approaches the value N_S= 3.1x10^{13} cm^{-2} calculated with a pure GaN buffer layer. The sensitivity of N_S on t_{GaN} is weaker in the region of 0.1-1.0 μm but it

should be always considered in the design of HEMT structures with a thin GaN buffer layer on AlN back barrier.

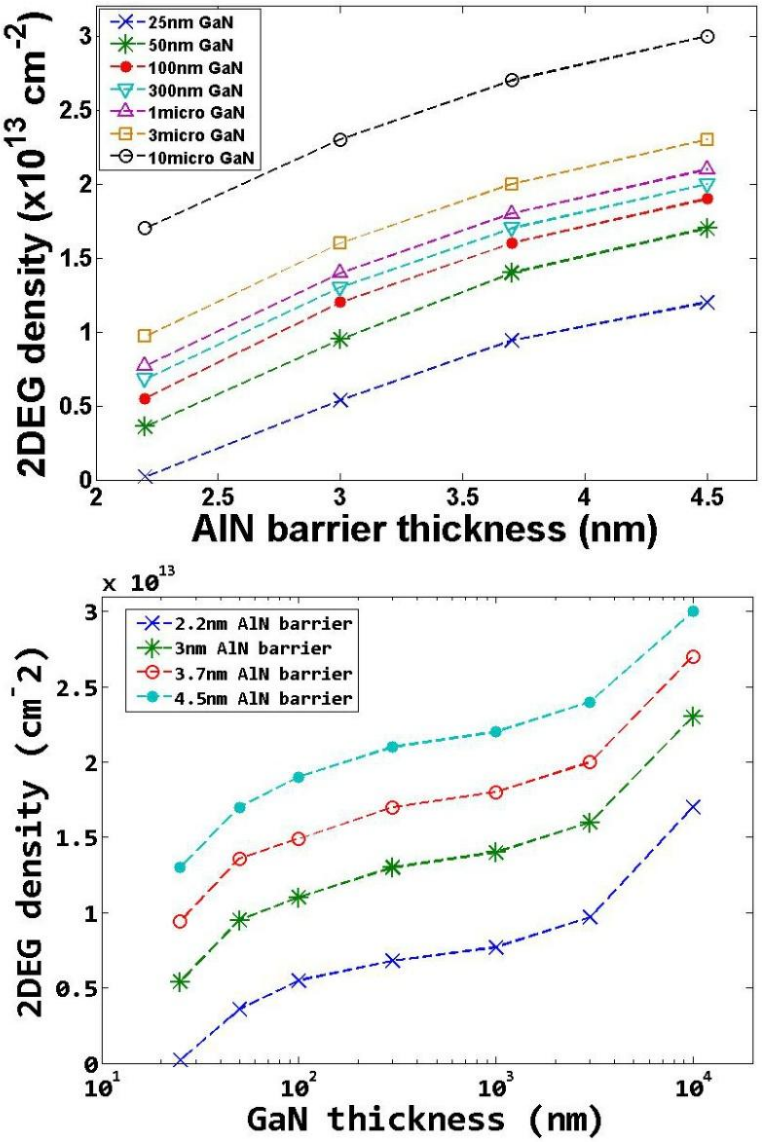

Fig. 5.12. (a) Calculated 2DEG density for structures [1nm GaN/ t_b(nm) AlN/ t_{GaN} nm GaN/ 200 nm AlN] versus AlN barrier thickness (t_b) in the range of 1.5-4.5 nm and for different GaN buffer layer thicknesses (t_{GaN}) in the range of 25nm-10μm. (b) Calculated 2DEG density for structures [1nm GaN/ t_b(nm) AlN/ t_{GaN} nm GaN/ 200 nm AlN] versus GaN buffer layer thickness (t_{GaN}) in the range of 25nm-10μm and for different AlN barrier layer thicknesses (t_b) in the range of 1.5-4.5 nm.[1]

It should be also noticed that at the bottom GaN/AlN interface the valence band crosses the Fermi level (Fig. 5.10 (a)[1]), which can cause an accumulation of holes of the order of 10^{13} cm^{-2}. The presence of the theoretically predicted two-dimensional hole gas (2DHG) would depend on the amount of defect-induced charges, which have been ignored in our SCSP calculations. An experimental determination of 2DHG has not become possible; similarly to a previous work on strained GaN QW channel AlN/GaN/AlN double barrier heterostructures.[15] In our thin heteroepitaxial structures, the bottom GaN/AlN interface is located at 200 nm above the highly lattice-mismatched sapphire substrate. Thus, a high defect density is expected that may compensate the polarization induced charges.

In conclusion, an interesting finding of this work is the excellent consistency of SCSP calculations, material/2DEG properties and HEMT device currents, although heteroepitaxial structures with a very thin GaN/AlN buffer layer on the highly lattice-mismatched sapphire substrates were investigated. This indicates a very good control and reproducibility of the heteroepitaxial growth process and the negligible impact of extended defects on the device electrostatics. The high density of polarization charge at the AlN/GaN interface dominates the properties of the structures that approach the ideal configuration of the SCSP calculations. The results were also confirmed by the performance of 1 μm gate-length transistors. The maximum drain-source current was 1.1 A/mm, for AlN barrier thickness of 3.0 nm and 3.7 nm, and the maximum extrinsic transconductance was 320 mS/mm for 3.0 nm AlN barrier.

References

[1] A. Bairamis, Ch. Zervos, A. Adikimenakis, A. Kostopoulos, M. Kayambaki, K. Tsagaraki, G. Konstantinidis & A. Georgakilas, *Appl. Phys. Lett.* **105**, 113508 (2014)

[2] Ch. Zervos, A. Adikimenakis, A. Bairamis, A. Kostopoulos, M. Kayambaki, K. Tsagaraki, G. Konstantinidis & A. Georgakilas, *Semicond. Sci. Technol.* **31**, 065002 (2016)

[3] T. Zimmermann, D. Deen, Y. Cao, J. Simon, P. Fay, D. Jena & H. G. Xing, *IEEE Electron Device Lett.* **29,** 661 (2008)

[4] A. Adikimenakis, K. E. Aretouli, E. Iliopoulos, A. Kostopoulos, K. Tsagaraki, G. Konstantinidis & A. Georgakilas, *Microelectron. Eng.* **86**, 1071 (2009)

[5] F. Medjdoub, M. Zegaoui, D. Ducatteau, N. Rolland & P. A. Rolland, *IEEE Electron Device Lett.* **32,** 874 (2011)

[6] S. L. Rumyantsev, N. Pala, M. S. Shur, and R. Gaska, M. E. Levinshtein, M. Asif Khan, G. Shin, X. Hu & J. Yang, *J. Appl. Phys.* **90**, 310 (2001)

[7] Y. Dora, A. Chakraborty, S. Heikman, L. McCarthy, S. Keller, S. P. DenBaars & U. K. Mishra, *IEEE Electron Device Lett.* **27**, 529 (2006)

[8] A. L. Corrion, K. Shinohara, D. Regan, I. Milosavljevic, P. Hashimoto, P. J. Willadsen, A. Schmitz, S. J. Kim, C. M. Butler, D. Brown, S. D. Burnham & M. Micovic, *IEEE Electron Device Lett.* **32,** 1062 (2011)

[9] G. Li, R. Wang, J. Guo, J. Verma, Z. Hu, Y. Yue, F. Faria, Y. Cao, M. Kelly, T. Kosel, H. Xing & D. Jena, *IEEE Electron Device Lett.* **35,** 661 (2012)

[10] Z. Y. Fan, J. Li, M. L. Nakarmi, J. Y. Lin & H. X. Jiang, *Appl. Phys. Lett.* **88**, 073513 (2006)

[11] Y.F. Wu, B.P Keller, S. Keller, D. Kapolnek, P. Kozodoy, S.P. Denbaars & U.K. Mishra, *Appl. Phys. Lett.* **69**, 1438 (1996)

[12] P. Herfurth, Y. Men, R. Rosch, J.F. Carlin, N. Grandjean & E. Kohn, *Phys. Status Solidi C* **9,** 945 (2012)

[13] P. Herfurth, D. Maier, L. Lugani, J.F. Carlin, R. Rosch, Y. Men, N. Grandjean & E. Kohn, *IEEE Electron Device Lett.* **34,** 496 (2013)

[14] L. Lugani, J. F. Carlin, M. A. Py, D. Martin, F. Rossi, G. Salviati, P. Herfurth, E. Kohn, J. Blasing, A. Krost & N. Grandjean, *J. Appl. Phys.* **113**, 214503 (2013)

[15] G. Li, B. Song, S. Ganguly, M. Zhu, R. Wang, X. Yan, J. Verma, V. Protasenko, H. G. Xing & D. Jena, *Appl. Phys. Lett.* **104**, 193506 (2014)

[16] M. Zervos, A. Kostopoulos, G. Constantinidis, M. Kayambaki & A. Georgakilas, *J. Appl. Phys.* **91**, 4387 (2002)

[17] A. Georgakilas, S. Mikroulis, V. Cimalla, M. Zervos, A. Kostopoulos, Ph. Komninou, Th. Kehagias & Th. Karakostas, *Phys. Status Solidi A* **188**, 567 (2001)

[18] S. Mikroulis, A. Georgakilas, A. Kostopoulos, V. Cimalla, E. Dimakis & Ph. Komninou, *Appl. Phys. Lett.* **80**, 2886 (2002)

[19] I-H. Tan, G. L. Snider, L. D. Chang & E. L. Hu, *J. Appl. Phys.* **68,** 4071 (1990)

[20] O. Ambacher, J. Majewski, C. Miskys, A. Link, M. Hermann, M. Eickhoff, M. Stutzmann, F. Bernardini, V. Fiorentini, V. Tilak, B. Schaff & L. F. Eastman, *J. Phys.: Condens. Matter* **14** , 3399 (2002)

[21] C. G. Van de Walle & J. Neugebauer, *Nature* **423**, 626 (2003)

[22] Y. Cao & D. Jena, *Appl. Phys. Lett.* **90**, 182112 (2007)

5.3 Surface passivation of AlN/GaN HEMT structures

As we have mentioned before, AlN/GaN heterostructures, due to the strong spontaneous and piezoelectric polarization of AlN, allow the formation of high density 2DEG at the AlN/GaN interface.[1] Although these structures with high 2DEG densities can be successfully grown,[2,3,4] the existing trapping effects may limit the performance of the fabricated devices through drain-current collapse.[5] The reduction of surface states and sheet resistance, which is favorable for a device operation, is feasible using different passivation layers or gate insulators (such as SiO_2, SiN_x, Al_2O_3, HfO_2 and AlN).[6-16] The excess of defect density at III-V oxide interfaces is a problem that is mainly caused by two reasons: the first is the strain, although there are oxides that do not create strain, and the second is the universal problem of large interface state density (D_{it}).[17]

We tried to provide an insight into GaN and AlN surface passivation, using an *in-situ* SiN_x cap layer grown by plasma-assisted molecular beam epitaxy (PAMBE). The HEMT structures (passivated and unpassivated) were analyzed both theoretically and experimentally, and the effect of SiN_x cap layer on the 2DEG density was evaluated.

5.3.1 Experimental Details and Calculations

Four metal-polarity AlN/GaN HEMT structures (A, B, C and D), with a thin 300 nm GaN/200 nm AlN buffer layer, were grown heteroepitaxially on insulating Al_2O_3 (0001) substrates by PAMBE, as shown in the Figure 5.13. The *unpassivated* HEMT structures (A, B) comprised of (from top to bottom): A) 3.5 nm AlN barrier/300 nm GaN buffer/200 nm AlN buffer-nucleation layer and B) 1 nm GaN/3.5 nm AlN barrier/300 nm GaN buffer/200 nm AlN buffer-nucleation layer. The *passivated* structures (C, D) were identical plus depositing a 5 nm SiN_x cap layer. The SiN_x layer was deposited in the MBE system at 250 °C using reactive nitrogen from a N_2 RF plasma source and Si from an sublimation cell. The substrate preparation and the nitridation conditions of all samples were according to the optimum conditions determined in previous works.[18,19] The growth of the 200 nm AlN nucleation-buffer layer on sapphire was carefully optimized, to provide a smooth surface for the overgrown layers.[2]

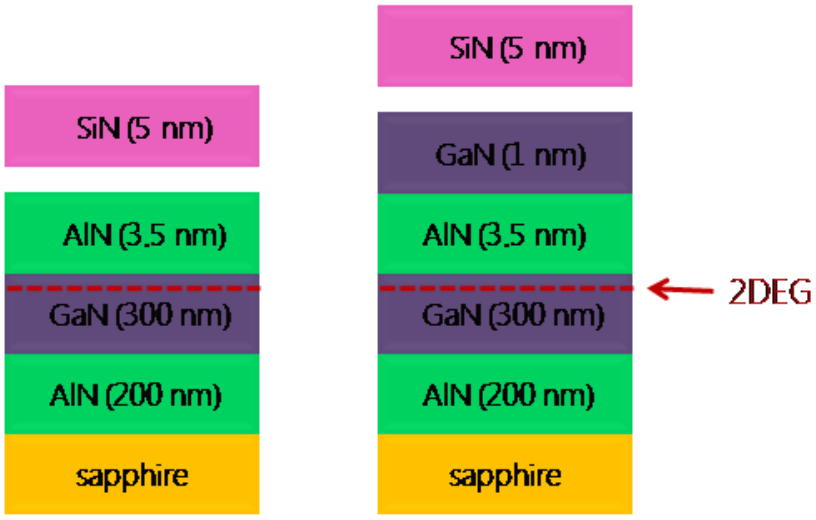

Fig. 5.13. Schematic illustration of the structures grown by PAMBE. The only difference between passivated and unpassivated heterostructures is the 5 nm SiN_x cap layer.

A self-consistent Schrödinger-Poisson (SCSP) solver[20] was employed to determine the equilibrium energy band profiles of the unpassivated and passivated structures and identify the effect of SiN_x cap layer thickness on 2DEG density. All relevant parameters, used in the calculations, were according to Ambacher et al.[21] The conduction band discontinuities, ΔE_C, were according to Van de Walle et al.[22] and according to Hashizume et al.[23] for AlN/GaN and SiN/GaN interfaces, respectively. For the boundary conditions, the energy distance $(E_C\text{-}E_F)_S$ between conduction band E_C and Fermi level (E_F) at the SiN (AlN, GaN) surface was set at 1.7 eV[6] (3.0 eV, 0.84 eV[21]), while neutrality was considered at the bottom side. The band gap energy of SiN was considered at 5.0 eV.[23] For donor concentrations, we assumed $N_D=7x10^{17}$ cm^{-3} for GaN, $N_D=10^{13}$ cm^{-3} for AlN and $N_D=10^9$ cm^{-3} for SiN_x. The impact of the in-situ SiN_x cap layer on the 2DEG properties was also studied through an analysis of resistivity and Hall-effect measurements, in order to evaluate our calculated results. Measurements were carried out at 300 K with a magnetic field of 0.4 T.

5.3.2 Results and Discussion

The strained AlN layer of an AlN/GaN structure has a positive polarization charge $+Q_p$ (which is the sum of the spontaneous and piezoelectric charges) at the AlN/GaN interface and a negative charge $-Q_p$ at the towards-the-surface side of the layer. In order to retain charge neutrality, we have to consider in our calculations a *positive fixed charge* $+Q_{fix.}$ which is equal to $+Q_p$ ($Q_{fix.} = Q_p$) (see Fig. 5.14(b)). Many groups have already demonstrated the case of a fixed charge in the oxide/III-nitride interface and have explained the physical origin of its existence.[6,7,10,14,24,25] Generally, the interfacial charge at an oxide/III-nitride interface includes contributions from fixed charge at the interface, interface trapped charge and positively-charged ionized surface donors.[10] Active interface trapped charge and ionized surface donors were neglected in our calculations and the fixed charge at the oxide/III-nitride interface, $+Q_{fix.}$, was used as the only charge fitting parameter. The density of the fixed sheet charge we considered in the calculations was $Q_{fix.} = Q^{AlN(tot.)} = \sigma^{AlN(tot.)}/e = 8.7\text{x}10^{13}$ cm^{-2} for the SiN_x/AlN interface and $Q_{fix.} = Q^{GaN(sp.)} = \sigma^{GaN(sp.)}/e = 2.3\text{x}10^{13}$ cm^{-2} for the SiN_x/GaN interface, where e is the electron charge and where $Q^{AlN(tot.)}$ and $Q^{GaN(sp.)}$ are the surface polarization charges of the strained AlN layer and relaxed GaN layer, respectively. The case of a GaN thin cap layer on a thin AlN barrier layer was considered.

The calculated conduction band (E_C) diagrams and electron distribution profiles of the AlN/GaN HEMT structure, with and without SiN_x passivation, are suggestively shown in Fig. 5.14 (a). It is clear that, the surface passivation with SiN_x deepens the 2DEG quantum well with corresponding increase of N_S. Figure 5.14 (b) shows the electrostatic charge distribution of the respective passivated structure.

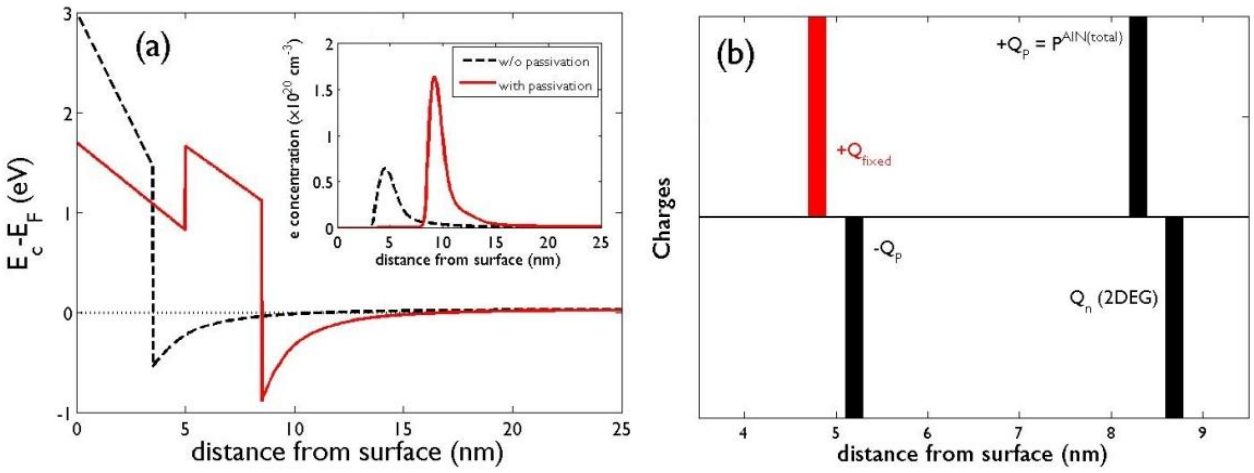

Fig. 5.14. (a) Simulated conduction band diagrams and electron distribution profiles for the top region of the structure [5 nm SiN_x/ 3.5 nm AlN/ 300 nm GaN], with (red solid line) and without (black dashed line) SiN_x passivation layer. (b) Electric charge distribution of the same passivated structure, where Q_{fixed} is the charge we considered in order to retain charge neutrality at the III-nitride surface.

Prior to the passivation, the AlN (GaN) surface has an excess of negative charge coming from the polarization induced charge $-Q_p$, which is present at the (AlN) GaN top surface. By depositing the SiN_x cap layer, these bound negative charges are compensated by the positive fixed charges at the dielectric/semiconductor interface. The more neutralization of the negative polarization charges of the III-nitride surface, by the positive sheet charge, the more increasing of the 2DEG density at the heterojunction. Comparative studies on electrical characteristics of AlGaN/GaN heterostructures with thin SiN_x films, deposited by different methods, have confirmed that SiN_x deposition increases N_S regardless of the deposition method.[26]

Moreover, SiN_x plays an important role to increase the breakdown voltage which is related with interface trapped electrons.[12] Other groups have suggested that, after passivation, due to enhancement of the strain, induced piezoelectric charge increases the sheet carrier concentration at AlGaN/GaN interface.[7]

The calculated 2DEG density, N_S, of $3.1x10^{13}$ cm^{-2} for the AlN/GaN HEMT structure (sample A), is significantly lower compared to $N_S = 4.7x10^{13}$ cm^{-2} calculated for the passivated one (sample C), as shown in Fig. 5.15 (a). This calculation shows that after 5-nm-SiN_x passivation, the 2DEG carrier density increases by approximately 51%. Respectively, for the GaN/AlN/GaN structure (sample B) we calculated $N_S = 2.7x10^{13}$ cm^{-2}, while for the passivated one (sample D) N_S was $3.5x10^{13}$ cm^{-2}, corresponding to an increase of about 29% (Fig. 5.15 (b)). These results are in a very good agreement with the values determined by Hall-effect measurements. Both unpassivated samples A and B exhibited $N_S = 3.0x10^{13}$ cm^{-2}, while the passivated samples C and D exhibited $N_S = 4.5x10^{13}$ cm^{-2} and $N_S = 4.3x10^{13}$ cm^{-2}, respectively.

Figure 5.15 (c) shows electron mobility decreasing after passivation with 5 nm SiN_x, for both structures. The non-passivated samples A and B exhibited mobilities of 590 and 740 cm^2/Vs, respectively. A relative reduction of mobility was observed in the passivated structures, reaching the values of 500 and 660 cm^2/Vs for samples C and D, respectively. This could be attributed to an increase in the interface roughness scattering, or maybe related to the diffusion of Si atoms into the III-nitride layers.[6]

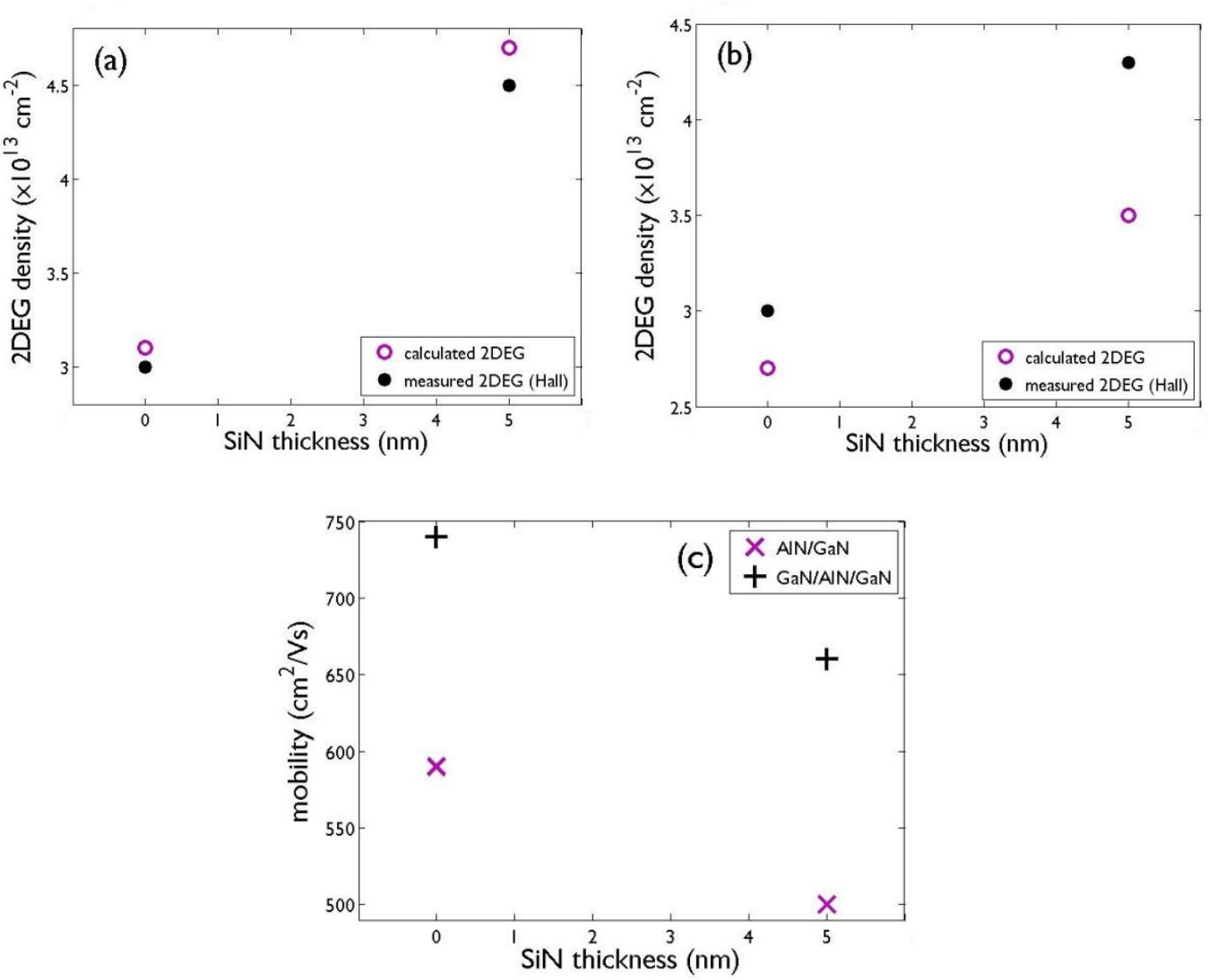

Fig. 5.15. Calculated (open circles) and experimental (solid circles) 2DEG sheet density (N_S), as functions of SiN_x passivation thickness (t_{SiN} = 0 and 5 nm), for structures (a) [t_{SiN} (nm)/ 3.5 nm AlN/ 300 nm GaN] and (b) [t_{SiN} (nm)/ 1 nm GaN/ 3.5 nm AlN/ 300 nm GaN]. (c) Electron Hall mobilities, as functions of SiN_x passivation thickness (t_{SiN} = 0 and 5 nm), for both structures.

To identify the role of the thickness of the SiN_x passivation layer on the III-nitride surface (we consider here the case of the strained AlN layer), combined with the presence (or absence) of the fixed sheet charge at the SiN_x/III-nitride interface, a series of SCSP calculations was carried out for the HEMT structure consisting of t_{SiN} (nm) SiN_x/ 3.5 nm AlN/ 300 nm GaN/ 200 nm AlN, where the SiN_x thickness (t_{SiNx}) was varied from 0 to 15 nm (0, 1, 5, 10 and 15 nm). The calculated N_S values have been plotted versus t_{SiN} in Fig. 5.16. The N_S increases with increasing t_{SiNx} and varies from $N_S = 3.1 \times 10^{13}$ cm^{-2} for $t_{SiNx} = 0$ nm (unpassivated case) to $N_S = 5.1 \times 10^{13}$ cm^{-2} for $t_{SiNx} = 15$ nm. As elsewhere,[6,7,14,24] a saturation tendency is observed in the increasing of N_S for SiN_x thicknesses above 15 nm.

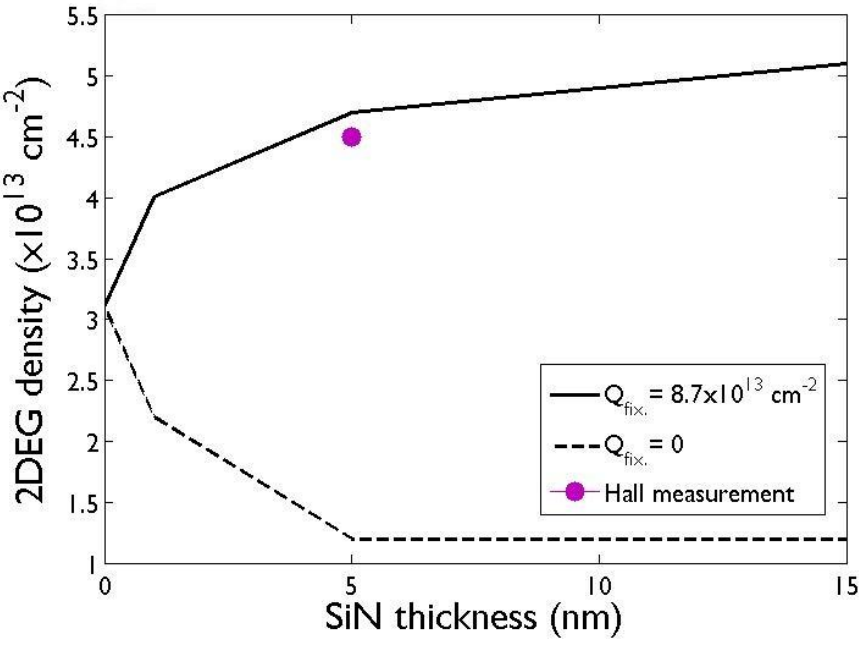

Fig. 5.16. Simulated 2DEG density (N_S) for structure [t_{SiNx} (nm)/ 3.5 nm AlN/ 300 nm GaN], for zero (dashed line) and non-zero (solid line) positive fixed charge (Q_{fix}), where t_{SiNx} = 0, 1, 5, 10 and 15 nm. The solid circle shows the value of N_S, measured by Hall-effect method, for t_{SiNx} = 5 nm.

In the same figure (Fig. 5.16), we have also plotted the same values for the case of $Q_{fix.} = 0$. In the absence of fixed sheet charge, a reduction of the N_S density is observed for increasing thickness of SiN_x. Characteristically, for $t_{SiNx} = 5$ nm we get $N_S = 1.2x10^{13}$ cm^{-2}, which is a value contradictory to the measured value from Hall-effect ($N_S = 4.5x10^{13}$ cm^{-2}). In that way, we confirm the need of considering a $Q_{fix.}$ in our calculations in order to agree with the experimental results. We tend to believe that the fixed positive charge in the oxide/III-nitride interface acts in a self-regulating way in order to retain charge neutrality. The results of Ganguly et al.[24] and Shealy et al.,[14] which show that the fixed charge is needed to passivate the surface of AlN and the surface of AlGaN, with an atomic layer deposited (ALD) Al_2O_3 and with a SiN_x layer, respectively, are almost equal to the polarization charges of the underlying III-nitride layer, maybe ratify this self-regulating passivation mechanism. Or even more, maybe neutralization of a III-nitride surface is independent from the species of the insulator, but this is something that needs further research in order to be claimed.

In conclusion, surface passivation of AlN/GaN HEMT structures, by *in-situ* SiN_x grown by PAMBE, has been analyzed theoretically and experimentally and the effect of passivation layer on 2DEG properties was evaluated. By depositing the SiN_x cap layer, the bound negative charges, which are present due to polarization effects, are compensated by the positive fixed charge in the dielectric with corresponding increase of 2DEG density. In order for theoretical results to agree with the experimental ones, we need to consider this fixed charge in our calculations. Taking into consideration the results of other groups, we tend to believe that the fixed positive charge in the oxide/III-nitride interface acts in a self-regulating way in order to retain charge neutrality, but more research in this direction is needed.

References

[1] O. Ambacher, B. Foutz, J. Smart, J. R. Shealy, N. G. Weimann, K. Chu, M. Murphy, A. J. Sierakowski, W. J. Schaff, L. F. Eastman, R. Dimitrov, A. Mitchell & M. Stutzmann, *J. Appl. Phys.* **87**, 334 (2000)

[2] A. Bairamis, Ch. Zervos, A. Adikimenakis, A. Kostopoulos, M. Kayambaki, K. Tsagaraki, G. Konstantinidis & A. Georgakilas, *Appl. Phys. Lett.* **105**, 113508 (2014)

[3] A. Adikimenakis, K. E. Aretouli, E. Iliopoulos, A. Kostopoulos, K. Tsagaraki, G. Konstantinidis & A. Georgakilas, *Microelectron. Eng.* **86**, 1071 (2009)

[4] Y. Cao & D. Jena, *Appl. Phys. Lett.* **90**, 182112 (2007)

[5] S. Arulkumaran, T. Egawa, H. Ishikawa & T. Jimbo, *Appl. Phys. Lett.* **81**, 3073 (2002)

[6] N. Maeda, M. Hiroki, N. Watanabe, Y. Oda, H. Yokoyama, T. Yagi, T. Makimoto, T. Enoki & T. Kobayashi, *Jpn. J. Appl. Phys.* **46**, 547 (2007)

[7] W. Wang, J. Derluyn, M. Germain, M. Leys, S. Degroote, D. Schreurs & G. Borghs, *Jpn. J. Appl. Phys.* **45**, L224 (2006)

[8] S. Arulkumaran, T. Egawa, H. Ishikawa, T. Jimbo & Y. Sano, Appl. Phys. Lett. **84**, 613 (2004)

[9] X. Z. Dang, E. T. Yu, E. J. Piner & B. T. McDermott, *J. Appl. Phys.* **90**, 1357 (2001)

[10] B. P. Downey, D. J. Meyer, D. S. Katzer, T. M. Marron, M. Pan & X. Gao, *Solid State Electron.* **106**, 12 (2015)

[11] J. Kuzmik, G. Pozzovivo, S. Abermann, J-F Carlin, M. Gonschorek, E. Feltin, et al., *IEEE Trans. Electron Devices* **55**, 937 (2008)

[12] J. Derluyn, S. Boeykens, K. Cheng, R. Vandersmissen, J. Das, W. Ruythooren, S. Degroote, M.R. Leys, M. Germain & G. Borghs, *J. Appl. Phys.* **98**, 054501 (2005)

[13] F. A. Faria, K. Nomoto, Z. Hu, S. Rouvimov, H. G. Xing & D. Jena, *J. Cryst. Growth* **425**, 133 (2015)

[14] J. R. Shealy, T. R. Prunty, E. M. Chumbes & B. K. Ridley, *J. Cryst. Growth* **250**, 7 (2003)

[15] Ch. Zervos, A. Adikimenakis, P. Beleniotis, A. Kostopoulos, M. Kayambaki, K. Tsagaraki, G. Konstantinidis & A. Georgakilas, *Appl. Phys. Lett.* **108**, 142102 (2016)

[16] Ch. Zervos, A. Adikimenakis, P. Beleniotis, A. Kostopoulos, M. Androulidaki, K. Tsagaraki, M. Kayambaki, G. Konstantinidis & A. Georgakilas, *J. Vac. Sci. Technol. B* **35**, 021210 (2017)

[17] J. Robertson, Y. Gao & L. Lin, *J. Appl. Phys.* **117**, 112806 (2015)

[18] A. Georgakilas, S. Mikroulis, V. Cimalla, M. Zervos, A. Kostopoulos, Ph. Komninou, Th. Kehagias & Th. Karakostas, *Phys. Status Solidi A* **188**, 567 (2001)

[19] S. Mikroulis, A. Georgakilas, A. Kostopoulos, V. Cimalla, E. Dimakis & Ph. Komninou, *Appl. Phys. Lett.* **80**, 2886 (2002)

[20] I-H. Tan, G. L. Snider, L. D. Chang & E. L. Hu, *J. Appl. Phys.* **68**, 4071 (1990)

[21] O. Ambacher, J. Majewski, C. Miskys, A. Link, M. Hermann, M. Eickhoff, M. Stutzmann, F. Bernardini, V. Fiorentini, V. Tilak, B. Schaff & L. F. Eastman, *J. Phys.: Condens. Matter* **14**, 3399 (2002)

[22] C. G. Van de Walle & J. Neugebauer, *Nature* **423**, 626 (2003)

[23] T. Hashizume, S. Ootomo, T. Inagaki & H. Hasegawa, *J. Vac. Sci. Technol. B* **21**, 1828 (2003)

[24] S. Ganguly, J. Verma, G. Li, T. Zimmermann, H. Xing & D. Jena, *Appl. Phys. Lett.* **99**, 193504 (2011)

[25] M. Esposto, S. Krishnamoorthy, D. N. Nath, S. Bajaj, T-H Hung & S. Rajan, *Appl. Phys. Lett.* **99**, 133503 (2011)

[26] M. Higashiwaki, Z. Chen, R. Chu, Y. Pei, S. Keller, U. K. Mishra, N. Hirose, T. Matsui & T. Mimura, *Appl. Phys. Lett.* **94**, 053513 (2009)

Chapter 6

Conclusions

Firstly, optimization of the design and growth of the single AlN/GaN HEMT heterostructure was aimed in order to achieve the optimal possible crystal quality and control of 2DEG properties. The effects of GaN cap layer and AlN barrier thickness have been evaluated, both theoretically and experimentally. HEMT structures with different AlN barrier layer thicknesses were then grown and their electrical properties (electron concentration and electron mobility) were determined by Hall-effect measurements. We saw that electron sheet density (N_S) increases almost linearly with AlN thickness and reaches very high values, up to 4.6 x 10^{13}cm^{-3}. At the same time, electron mobility is reduced from 1500 cm^2/Vs (for 2.2 nm AlN) to ~1000 cm^2/Vs for a maximum AlN thickness of 4.5 nm. For higher AlN thicknesses, mobility decreases sharply, due to the formation of micro-cracks.

Subsequently, double AlN/GaN HEMT heterostructures with thin GaN/AlN buffer layer have been analyzed theoretically and experimentally and the effects of the back AlN barrier on 2DEG properties have been evaluated. HEMT structures consisting of 300nm GaN/ 200nm AlN buffer layer on sapphire were grown by PAMBE and exhibited a remarkable agreement with the theoretical calculations, which indicates a very good control and reproducibility of the heteroepitaxial growth process. The high density of polarization charge at the AlN/GaN interface dominates the properties of the structures that approach the ideal configuration of the SCSP calculations. The results were also confirmed by the performance of 1 μm gate-length transistors.

The maximum drain-source current was 1.1 A/mm, for AlN barrier thickness of 3.0 nm and 3.7 nm, and the maximum extrinsic transconductance was 320 mS/mm for 3.0 nm AlN barrier showing that the impact of extended defects on the device electrostatics was negligible.

Finally, surface passivation of AlN/GaN HEMT structures, by *in-situ* SiN grown by PAMBE, has been analyzed theoretically and experimentally and the effect of passivation layer on 2DEG properties was evaluated. By depositing the Si_xN_y cap layer, the bound negative charges at the III-nitride surface, which are present due to polarization, are compensated by positive fixed charge at the dielectric/III-nitride interface, with corresponding increase of 2DEG density. In order for theoretical results to agree with the experimental ones, we need to consider this fixed charge in our calculations. Taking into consideration others' groups results, we tend to believe that the fixed positive charge in the oxide/III-nitride interface acts in a self-regulating way in order to retain charge neutrality, but more research in this direction is needed.

❖